UNIVERSITA' DEGLI STUDI DI MILANO
Facoltà di Medicina e Chirurgia
Dipartimento di Biotecnologie Mediche e Medicina Traslazionale

Scuola di dottorato in Scienze Biomediche Cliniche e Sperimentali

Corso di dottorato
Biotecnologie Applicate alle Scienze Mediche (XXVII°ciclo)

Post-transcriptional and post-translational regulation of LSD1 in mammalian brain

TUTOR:
Prof.ssa Elena Battaglioli

COORDINATORE:
Prof. Massimo Locati

Tesi di dottorato di:

Emanuela TOFFOLO

Anno Accademico 2013/2014

INDEX

INTRODUCTION

1. Epigenetics and neuronal function

Emerging evidence indicates that post-transcriptional gene regulation is necessary for neuronal functions at several levels: by increasing proteome diversity through alternative splicing, or by enabling activity-dependent regulation of mRNA localization, translation or degradation in the dendrite (Ule and Darnell, 2006). Since our phenotype is the product of continuous gene–environment interactions, environmentally regulated intracellular signals constantly modulate gene transcription in order to obtain cellular plasticity. The capacity to mastermind such adaptation to circumstances relies on the possibility of neurons and glia to change their genomic structure in a replication independent manner (Fig. 1). A great number of accumulating evidences suggests that there is much more than DNA sequence that permits the brain to reorganize itself, and one way that such phenotypic plasticity can be established is through epigenetic mechanisms (Borrelli et al, 2008). Epigenetics refers to heritable changes in gene expression that are unrelated to variation in DNA sequence (Meaney et al, 2010). In the brain, where most neurons are post-mitotic, epigenetic represents the molecular interface mediating interactions between gene and environment and regulates complex functions such cognition, behaviour and language. The epigenome has therefore a homeostatic role, that is at the base of the transcritional plasticity that translate environmental stimuli into morphological and functional changes.

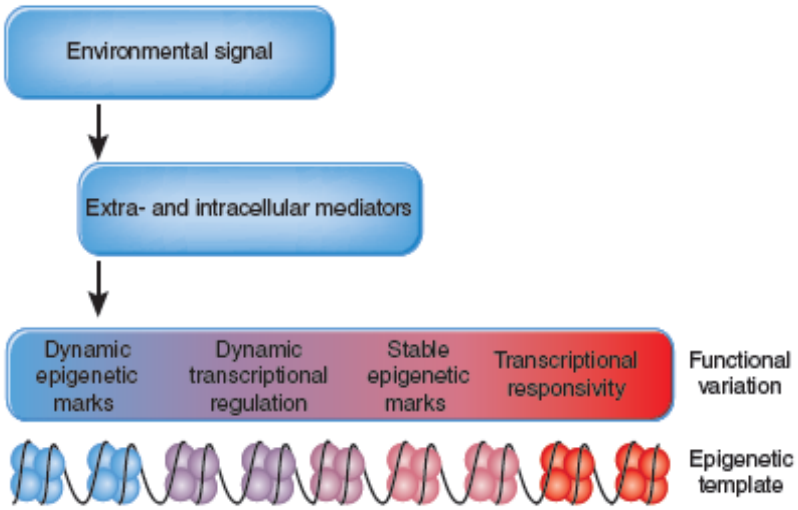

Fig. 1 The epigenetic interface. Epigenetic states lie at the interface between environmental signals and genome, serving to govern dynamic changes in transcriptional activity through extra- and intra-cellular mediators. In a multistep process, the epigenetic template attracts specific effectors that determine the responsivity of specific genomic regions to environmentally induced intracellular signaling pathways, thus leading to more stable effects on the potential of transcriptional activation and variation in neural function (color-graded region) (from Vasquero et al, 2003)

On the other hand, for the same reason the epigenome is vulnerable and chronic or strong acute insults of different origin for instance metabolic or stress factors, can stably modify the epigenetic asset generating the so called epigenetic "scars" that could have a pathogenic relevance. For al the above reasons, epi-pharmacological manipulation of chromatin remodeling pathways could be a novel approach in the treatment of several human disorders.

1.2 Histone modifications

The N-terminal tails of histones contain flexible and highly basic 15-30 aa-long sequences that are generally conserved across eukaryotic organisms and it is well established that they act as substrates for several types of post-translational modifications, including acetylation, methylation, ADP-ribosylation, ubiquitylation, and phosphorylation (Fig. 2) (Vasquero et al, 2003). Histone modifications are proposed to affect chromosome function through at least two distinct mechanisms. The first mechanism suggests that modifications may alter the electrostatic charge of the histone, causing structural changes or alteration of its DNA binding affinity. The second mechanism proposes that these modifications represent binding sites for protein recognition modules, such as the bromodomains or chromodomains, that bind acetylated lysines or methylated lysine, respectively (Cosgrove et al, 2004).

1.3 Histone H3 post translational modifications (PTM)

At the level of N-terminal tail of H3 a great number of PTMs have been identified: serine and threonine residues are well-known phospho-acceptor sites, while lysine and arginine residues have multiple choices of post-translational modification possibilities (Fig. 2). Lysine residues can be mono-, di-, or trimethylated at the z-amine in vivo. Recent genomic-scale analysis of histone modifications allows for general correlations between different H3K4 methylation states, their genomic loci, and gene expression levels. The emerging consensus is that high levels of H3K4 trimethylation are associated with the 5' regions of virtually all active genes and that there is a strong positive correlation between this modification, transcription rates, active polymerase II occupancy, and histone acetylation.

Fig 2 Schematic diagram of the covalent post-translational modifications (PTMs) of the histone H3 N-terminal tail. The different Histone H3 modifications are indicated (P, phosphorylation, shown in orange; Ub, ubiquitylation, shown in purple; Ac, acetylation, shown in blue; S, sumoylation, shown in yellow; N, neddylation, shown in pink). Methylation (Me) is shown on top, with green and red indicating the methyl marks that are associated with activation or repression, respectively.

2 HISTONE DEMETHYLASE LSD1/KDM1

2.1 Flavin-dependent histone demethylases

The discovery of Lysine Specific Demethylase 1 (LSD1) introduced a new concept in the field of the histone methylation, clearing the way for the idea that histone demethylation is possible. After LSD1 finding, many studies have been done and mechanisms for direct histone demethylase reactions have been proposed. Depending on the catalysis reaction, histone demethylases are subdivided in two main families: Flavin-dependent histone demethylases and Jumonji domain-containing demethylases (Culhane et al, 2007). As shown in figure 3, the Flavin-dependent histone demethylases, cause the oxidative cleavage of the C-N methyl group bond, coupling it with a two-electron reduction of the Flavin Adenine Dinucleotide (FAD) cofactor. This reaction produces an imine intermediate that is then non-enzymatically hydrolyzed. The methyl group is released as formaldehyde. This proteins exhibit specificity in the Lysine substrate, indeed they preferentially demethylate mono- and di-methyl Lysines. Since LSD1 is a good model for this protein family, their structure and function will be discussed later (Culhane etal, 2007).

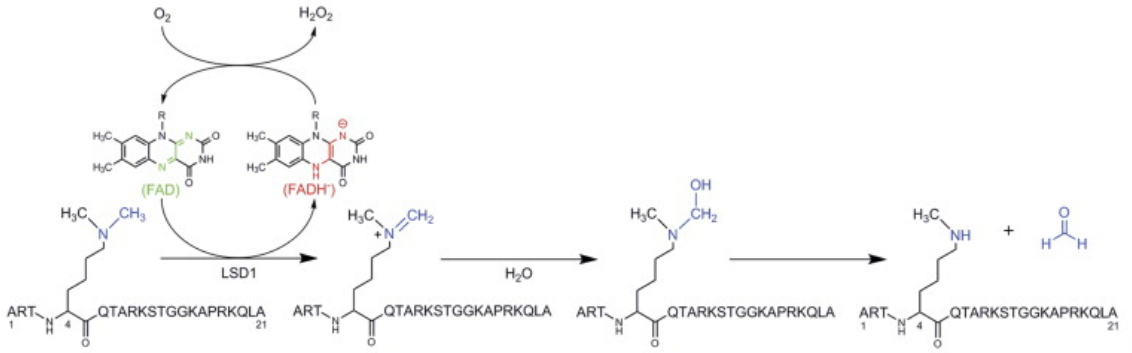

Fig 3 Catalytic mechanisms of FAD-dependent demethylase enzymes.
The FAD-dependent demethylation of Lys-4 of histone H3 proceeds through the hydrolysis of an iminium ion following a two-electron oxidation of the amine by the flavin. R, ribosyl adenine dinucleotide (from Culhane et al, 2007)

2.2 Lysin Specific Demethylase 1

Lysine Specific Demethylase 1 (LSD1, also named KMD1A or AOF2), is a flavin-dependent histone demethylases, that specifically acts on mono- or dimethylated lysine 4 on histone 3 (H3K4). Its function is predominantly related to gene repression, in fact it is required for downregulation of neuronal genes in non-neuronal cells. LSD1 demethylases function can also be related to different biological processes, such as development, cancer and neurological disorders. The human LSD1 protein is 852 aa long and consists of different domains (Fig. 4):

- N-terminal domain, composed of the SWIRM domain (involved in proteins interactions) and of an unstructured region made of linear motifs that might represent functional sites responsible for the association of LSD1 with different transcriptional protein complexes;
- C-terminal amine oxidase domain (AOD), composed of a substrate-binding portion and a FAD-binding portion. The enzyme active site is located between these two regions;
- "Tower Domain", made of two long antiparallel α- helices that project away from the globular AOD. This domain provides the interface for CoREST binding.

The histone tail adopts a folded conformation when bound to the enzyme and slides into the substrate-binding domain cavity, establishing a network of specific interactions with the active site residues. These interactions are important to correctly position the Lys4 in front of the FAD (Mosammaparast and Shi, 2010; Forneris et al, 2009). The LSD1 core complex contains LSD1, the proteins HDAC1, HDAC2 and CoREST. CoREST is a co-repressor protein that binds the neuronal Responsive Element RE1 Silencing Transcription factor (REST). Indeed LSD1

complex is recruited by REST through the direct binding to CoREST, resulting in the repression of neuronal genes in non-neuronal cells. The presence of CoREST in the complex is also important for the substrate binding and recognition: the C-terminal SANT domain of CoREST facilitates the association with chromatin by directly interacting with DNA. HDAC 1 and 2 deacetylate histone H3, allowing the binding of CoREST to the nucleosome and the LSD1 recruitment. Thus, the presence of HDAC1 and 2 suggests a coordinate modification of histone tails (Foster et al, 2010). Even if the active site of LSD1 is large enough to accommodate also H3K4me3, LSD1 demethylates only mono-or dimethylated H3K4, suggesting that the methyl state selectivity is not structurally inhibited but is chemically constrained, as predicted by its enzymatic mechanism. Some studies demonstrated that certain H3 tail modifications (such as acetylation on Lys 9 or phosphorylation on Ser 10) affect LSD1 activity, suggesting that LSD1 could act after the addiction or removal of other charge-altering histones modifications. Moreover, these findings suggest also that LSD1 complex is capable to read the histone code.
It has also been demonstrated that LSD1 complex function is not limited to REST-regulated neuronal genes, but it can be extended to other contexts. Thus, LSD1 can either repress or activate target genes through interacting with a variety of co-factors. For instance, there are some evidences that LSD1 can demethylate H3K9me2/me1, with an activating function. Indeed, it has been demonstrated that LSD1 directly binds the androgen receptor, and in this molecular complex is able to demethylate H3K9, functioning as a transcription activator. Anyway, it is still unclear how LSD1 changes its demethylase specificity when it engages different interacting partners Mosammaparast and Shi, 2010. It's a given that LSD1 also interacts with other proteins, including Carboxyl-terminal binding protein (CtBP), HMG domain containing protein BRAF35 and PHD-finger containing protein BHC80 (Foster et al, 2010). These proteins can enhance the HDAC1-2 activity, adding further regulatory steps to the LSD1 activity (Lee et al, 2005).

2.3 Neuronal LSD1 isoform: expression and activity

Given the central role of LSD1 in chromatin remodeling, in my laboratory the process of LSD1 alternative splicing was investigated in order to find out an additional mechanism of LSD1 regulation. This approach led to the discovery of 4 different LSD1 splicing isoforms (Fig. 4), deriving from combinatorial retention of two alternative exons: exon E2a and exon E8a. E2a is 60-bp-long and encodes for 20 aa, whereas the E8a is 12-bp-long and is translated into 4 aa with

sequence Asp-Thr-Val-Lys (Zibetti et al, 2010).

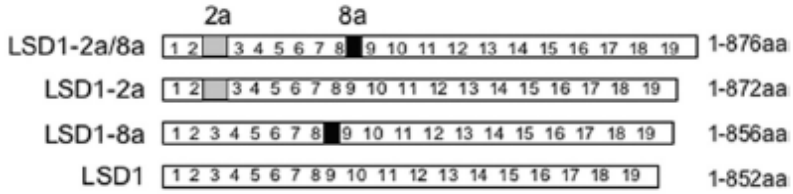

Fig. 4 Structure of the four LSD1 variants: single or double inclusion of two alternatively spliced exons, E2a and E8a, generates 4 different mammalian specific splicing variants (from Zibetti at al, 2010)

The inclusion of the two exons does not alter the reading frame and results in a protein of 876 aa. In this isoform, the amino acids coded by the exon E2a localize between the N-terminal disordered region and the SWIRM domain; whereas the four residues of the exon E8a immediately precede the CoREST-binding tower domain, which is inserted within the amine oxidase domain (Fig. 5). Both the two alternatively spliced introns present a very high conservation degree between human and mouse, a typical feature of alternatively spliced exons.

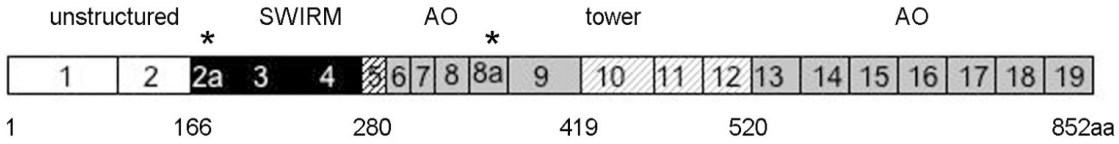

Fig. 5 Genomic organization of human LSD1 gene
Schematic representation of the human LSD1 protein domains together with its exons ranging from 1 to 19; asterisks indicate the location of annotated alternative exons (E2a and E8a). Different colors indicate functional domains. N-terminal unstructured region coded by exons 1–2, SWIRM domain coded by exons 2– 4, the SWIRM-oxidase connector coded by exon 5, the amine oxidase domain coded by exons 6–9 and exons 13–19, and the tower domain coded by exons 10 –12 (from Zibetti at al, 2010)

The isoforms containing exon E2a are ubiquitously expressed, as the wild type isoform is, whereas the isoform containing the sole exon E8a is restricted to the nervous system. Finally, the LSD1-E2a/8a isoform is expressed both in human brain and testis. It is interesting to note that while the E2a isoform is present in different species, such as lizard, chicken and mammals, the E8a isoforms are expressed only in mammals. Moreover, while the epigenetic factors are mostly ubiquitous, LSD1-E8a is one of the very few factors restricted exclusively to neurons. All the 4 splicing variants retain the ability to generate functional proteins and to form an active complex with CoREST and HDAC1-2. Biochemical *in vitro* assays using histone H3 peptides as substrate revealed that all three LSD1 isoforms bound to CoREST can demethylate Lys4 of histone H3

with a catalytic efficiency virtually identical to that displayed by wild type LSD1. Such unchanged enzymatic activity and substrate specificity is supported by a very similar three-dimensional structure, indeed even in the presence of exon E2a the N-terminal region of LSD1 remains unstructured, at least in the crystalline state. Also the overall conformation of LSD1-E8a is very similar to that of the native protein, since the neurospecific E8a residues Asp-Thr-Val-Lys form a sort of protrusion that emerges from the amino-ossidase domain of the protein but doesn't contact the histone peptide and CoREST (Fig. 6). From a functional point of view, the presence of the neuronal mini-exon E8a determines a significantly reduced repression of the Luciferase reporter gene activity (Zibetti et al, 2010). Moreover it was demonstrated that a fine balance of LSD1 isoforms allows differentiating neurons to acquire a proper morphology. Indeed, the expression of LSD1 splice variants is dynamically regulated during mammalian brain development and synaptic maturation, in particular during the perinatal stages. At early all the splicing isoforms are detectable, but the preponderal ones are LSD1 and LSD1-E2a. During the perinatal window, however, a rapid inversion of the proportions occurs, with a notable increase of the neuronal exon E8a containing isoforms and a decrease of the exon E2a isoforms. Exon E8a expression increases concomitantly with early stages of synaptogenesis, suggesting its implication during morphogenesis, possibly regulating the proper timing of neurite maturation. Nevertheless, after day P7, all LSD1 isoforms reach comparable levels, as it is possible to detect in adult mouse brain. Thus, LSD1 expression profile suggests a possible implication of neurospecific E8a-containing isoforms in neuronal development.

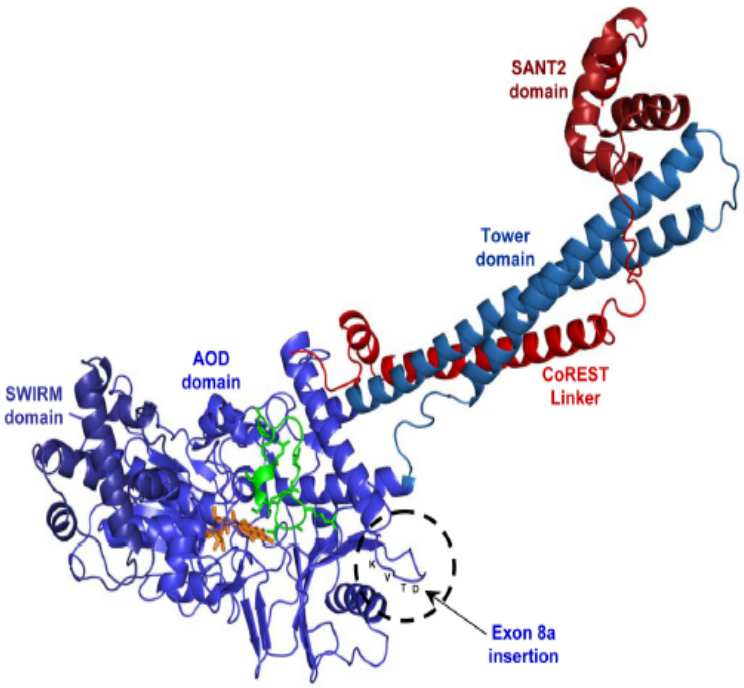

Fig. 6 Structure of neuroLSD1 splice variant/CoREST in complex with H3 peptide

*R*ibbon diagram of the structure. NeuroLSD1 is in *blue*, CoREST in *red*, and the peptide in *green*. The FAD cofactor is shown as a *yellow ball-and-stick*. The final model consists of residues 171–836 of LSD1, residues 308–440 of CoREST, and residues 1–16 of pLys4Met peptide. The insertion site of E8a (residues Asp369A-Thr369B-Val369C-Lys369D) is highlighted

2.4 The balance of LSD1/neuroLSD1 in the brain

Because inclusion of E8a is a neurorestricted event, its functions within CNS were initially been inferred by relating its expression profile to peculiar stages of neuronal differentiation (Zibetti et al, 2010). Time course analysis of the relative amount of each LSD1 splice isoform was performed by rqf-PCR in rat cortical tessues (which represent a suitable model of neuronal maturation) collected at several developmental stages. This analysis demonstrated an increase in neuro-LSD1 isoform between E18.5 and P1 compared to LSD1 and showed that this ratio remains stable along subsequent stages of development (Fig. 7). A parallel analysis showed that several synaptic markers arise during the perinatal window with a progressive increase over developmental stages, indicating that the inclusion frequency of E8a increases concomitantly with early stages of synaptogenesis.

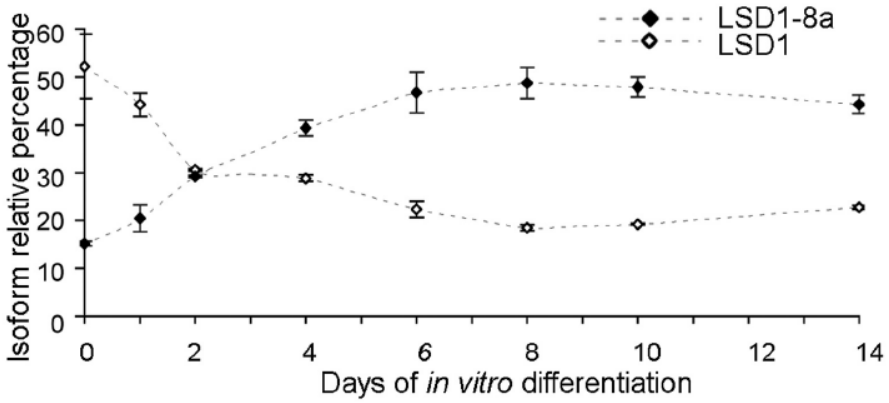

Fig. 7 LSD1 splicing analysis in a rat cortical neuron maturation system (From Zibetti at al, 2010)

LSD1 expression profile suggested immediatly a possible implication of neurospecific E8a-containing isoforms in neuronal development. To test this hypothesis, the expression of LSD1 isoforms within rat cortical neurons was perturbed in a developmental window important for synaptic maturation. To infer the function of LSD1 isoforms within neurons, they were knocked down differentially by generating short hairpin RNAs (shRNAs) specific for either neurospecific exon E8a or the splice junction between exon E8 and E9, which is shared among ubiquitous LSD1 isoforms (Zibetti et al, 2010). Phenotypic traits that describe neuronal morphogenesis during in vitro maturation, including cumulative neurite length, the number of branches, and neurite, were evaluated. The knockdown of ubiquitous isoforms ensued no effect when compared

with control according to cumulative neurite arborization, branch count, and neurite width. Conversely, the silencing of neurospecific isoforms altered neurite morphogenesis by eliciting a significant decrease of the cumulative neurite arborization (Fig. 8D), a reduced number of secondary branches (Fig. 8E), and a reduced average neurite width (Fig. 8F). Furthermore neurite morphogenesis after overexpressing LSD1 neurospecific isoforms was evaluated, because this was expected to exert opposite effects to those observed during knockdown experiments. Although the knockdown of neurospecific LSD1 isoforms delays neurite morphogenesis, overexpression of the same seems to anticipate features that normally arise at later stages under physiological conditions. Therefore only the change in the amount of neurospecific NeuroLSD1 isoform is able to alter neurite morphogenesis in terms of cumulative neurite arborization, number of secondary branches and average neurite width (Zibetti et al, 2010).

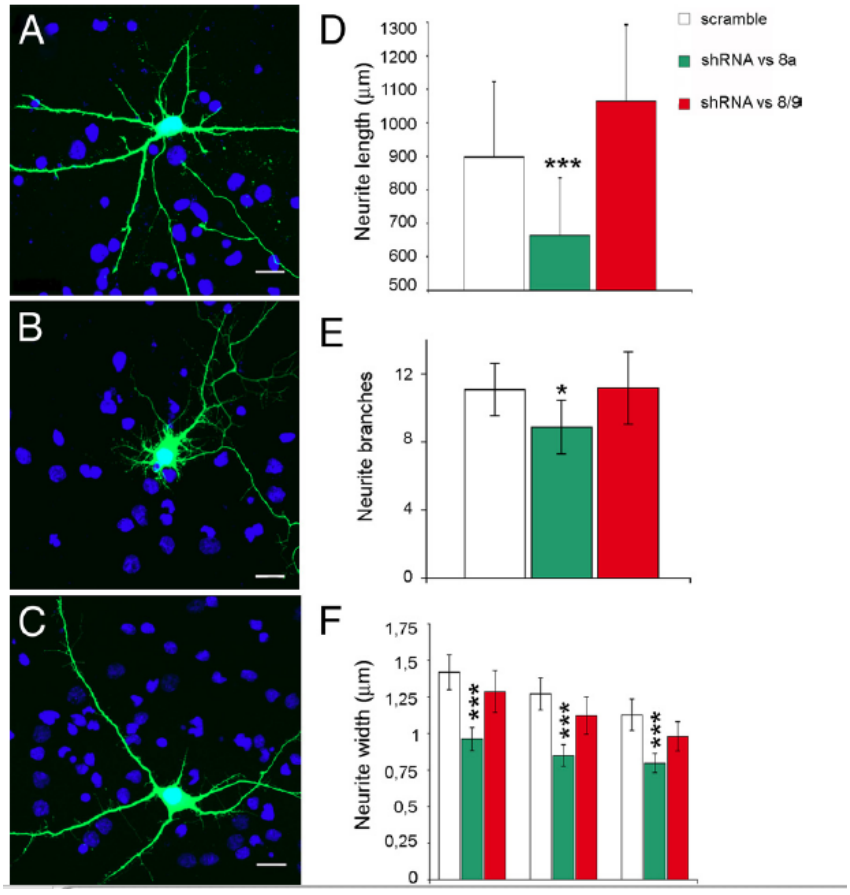

Fig. 8 Effect of neurospecific or ubiquitous LSD1 knockdown by shRNAs on neurite morphology in rat cortical neurons (from Zibetti et al, 2010)

3 UNDERSTANDING LSD1 NEUROSPECIFIC ALTERNATIVE SPLICING

The dynamically regulated expression of neuro-LSD1 within neuronal maturation and its implication in neuronal morphogenesis, suggested an important role for LSD1/neuroLSD1 balance in the CNS. This address the studies intended to understand the basis of neurospecific LSD1 splicing in vivo and its reliance on neuronal activity.

3.1 NeuroLSD1 splicing variant is transiently downregulated during neuronal activation

To understand whether in adult brain LSD1/neuroLSD1 ratio could be dynamically regulated in response to experience, different paradigms of neuronal activation were used (Rusconi et al, 2014). The pilocarpine-induced status epilepticus (PISE) entails strong activation of hippocampal circuitry. 5-week-old C57BL/6 mice with pilocarpine (i.p.) were treated using strandard procedures and behavioral observations addressing status epilepticus (SE), number, and severity of seizures were performed, in parallel with LSD1 splicing isoform quantification obtained by relative quantity fluorescence RT-PCR (rqfRT-PCR). It was observed an activity-dependent downregulation restricted to exon E8a splicing. Such change in the relative levels of the LSD1 isoforms was transient and by 24 h neuroLSD1 and LSD1 isoform levels were similar to controls (Fig. 9).

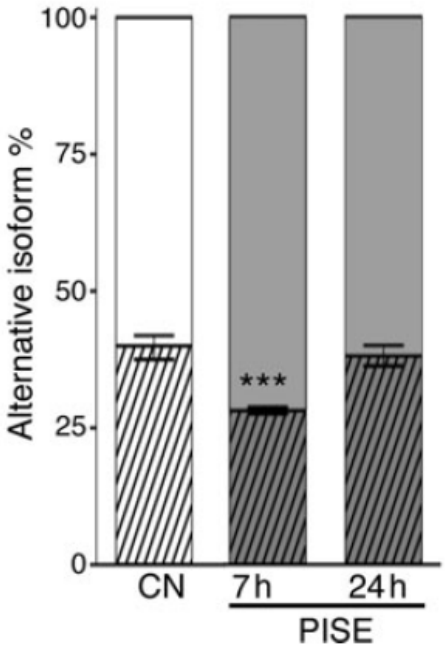

Fig. 9 Neuronal activation in vivo induces LSD1 exon E8a splicing downregulation. PISE was elicited in 5-week-old C57BL/6 mice. Seven or 24 h after the onset of status epilepticus hippocampal RNA was analyzed (n=10 mice per condition) and compared with control condition (from Rusconi et al, 2014)

3.2 NOVA1 and nSR100 participate in the regulation of exon E8a splicing

Since in a previous in vivo study aimed at the identification of NOVA splicing regulatory network, LSD1 exon E8a has been reported to be physically associated with NOVA proteins (Zhang et al, 2010), in our laboratory we had tried to provide mechanistic evidence that NOVA1 regulates LSD1 neurospecific alternative splicing (Rusconi et al, 2014). These experiments took advantage from Minigene assay, an assay to assess alternative splicing in cells. In order to identify the splicing regulatory elements in pre-mRNA and the proteins that bind these elements, minigenes are constructed that contain the alternatively spliced region and flanking genomic regions.

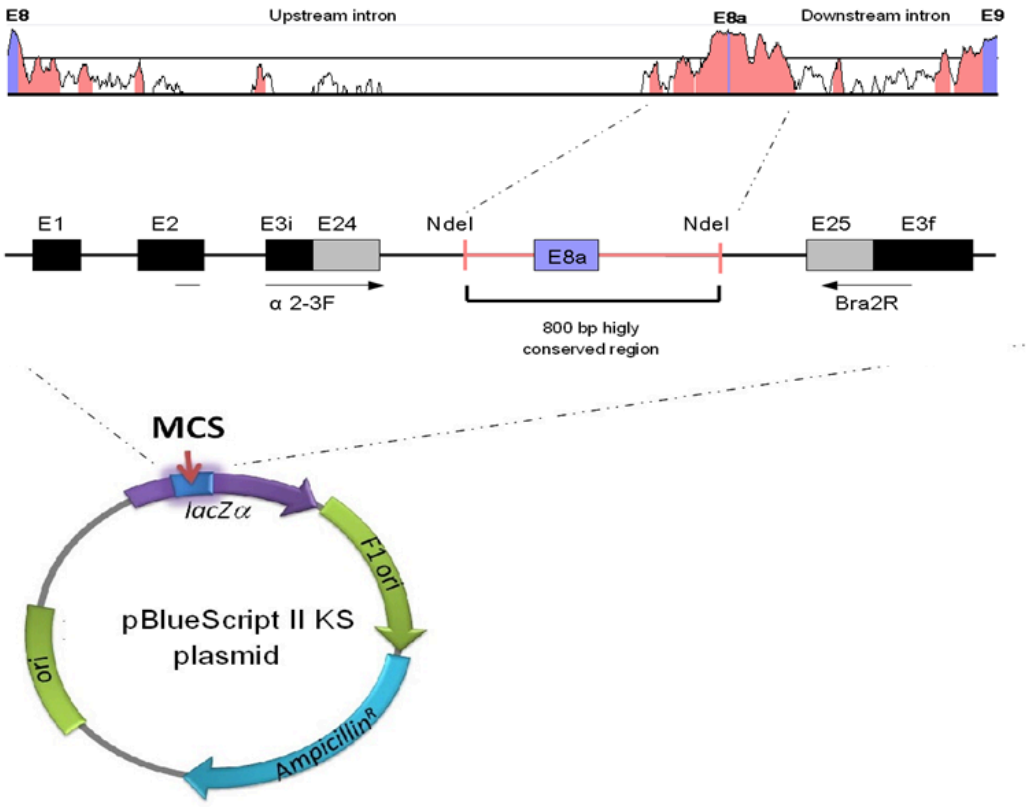

Fig.10 Schematic representation of the splicing vector pBS II KS with its multiple cloning site. In the minigene the exon 8a together with its intronic regions upstream and downstream (for about 800 bp) was cloned. NdeI cloning site was used for cloning.

The use of a minigene (MG) reporter assays, in wich 800 bp fragment including exon E8a and the highly conserved flanking intronic regions (hLSD1- MG800) was cloned, allowed to understand the role of NOVA1 in regulating LSD1 spicing in SH-SY5Y and HeLa cells.

Figure 11 shows how by cotransfecting hLSD1-MG800 along with increasing amount of NOVA1 we obtained a dose-dependent increasein exon E8a inclusion frequency in SH-SY5Y cells and no exon E8a inclusion in HeLa cells, even at the highest dose. Consistently with its ability to bind LSD1 transcripts (Zhang et al. 2010), NOVA1 actively participates in the regulation of exon E8a splicing.

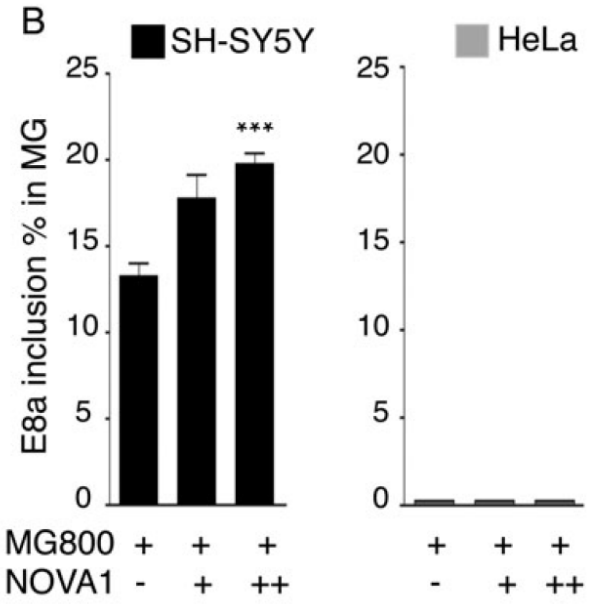

Fig. 11 NOVA1 regulates exon E8a splicing inclusion (from Rusconi et al, 2014)

The level of NOVA protein in hippocampus of mice treated with PISE, was analyzed, to understand if NOVA1 could be responsible for the decrease in exon E8a splicing inclusion triggered by PISE. As shown in figure 13, upon PISE, global NOVA1 protein levels and mRNA were reduced by about 30%, suggesting that hippocampal NOVA transcription is sensitive to electrical activity and is downregulated in response to PISE. Altogether, these findings suggest that, NOVA1 downregulation in response to PISE could account for the concomitant reduction of exon E8a inclusion frequency into LSD1 mature transcripts.

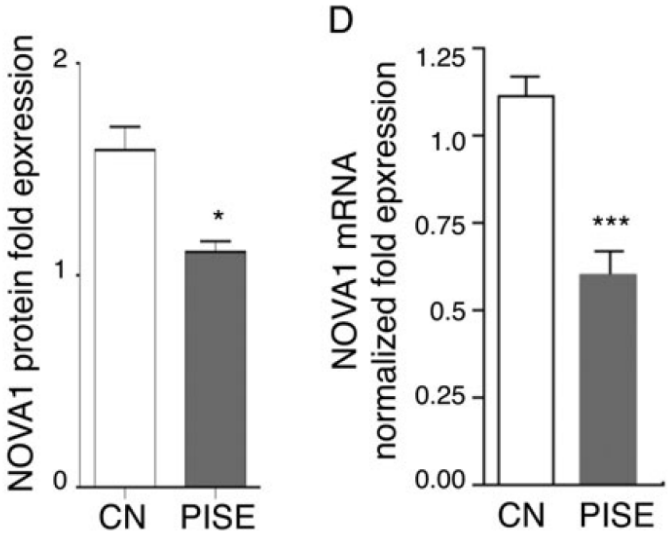

Fig 12 NOVA1 mRNA expression level from treated and control mice (from Rusconi et al, 2014)

NOVA1 is able to modulate exon E8a inclusion into MG-derived transcripts in a neuronal context but it is not sufficient to trigger splicing inclusion in HeLa cells. This suggests that NOVA1 is not directly responsible for restricting exon E8a splicing to the nervous system. In order to identify cis-acting elements regulating tissue-specific alternative splicing of LSD1 transcripts, a deletion analysis was performed. Deletion of the 450 bp located at the 3′ resulted in a dramatic increase of exon E8a inclusion in SH-SY5Y (up to 70% of the mature MG transcripts), indicating the presence of a strong negative cis-acting element within the removed fragment. A palindromic 21-bp element containing the reverse complement of exon E8a was identified by computer-assisted analysis of the deleted region. This palindrome is 100% conserved among mammals and maps about 300 bp downstream of exon E8a. Given its perfect complementarity to exon E8a, at the pre-mRNA stage, this region could trap the mini-exon and its donor and acceptor splicing sites into a perfect 21-bp-long double-stranded RNA structure (Fig. 13) hampering the splicing process.

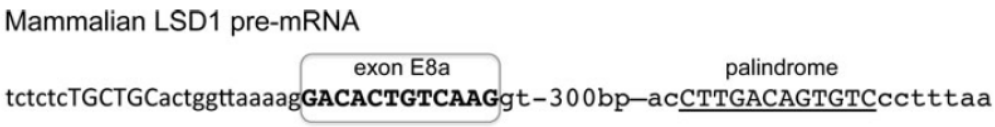

Fig.13 Representation of the palindromic 12 base-pair core sequence

Consistently, deletion of the 12-bp core sequence complementary to exon E8a from the palindrome resulted in a massive increase of exon E8a inclusion (85% of total MG transcripts). These data suggest that the palindromic element acts as a cis-silencer of exon E8a splicing in neuronal cells. However, as removal of this element was not sufficient to allow exon E8a inclusion in HeLa cells, it was postulated that, besides NOVA1, another neurospecific transacting factor is required to trigger E8a splicing. Among a subset of tissue-specific RNA binding factors (Braunschweig et al. 2013), namely nPTB, RB-FOX1, SAM68, and nSR100, only SR protein nSR100 (also known as SRRM4) was able to drive exon E8a inclusion in non-neuronal cells, not only into MG hLSD1-MG800 transcripts, but also into endogenous LSD1 transcripts, in a dose dependent manner, indicating nSR100 as necessary and sufficient factor to regulate LSD1 neurospecific splicing. SR proteins are so called because of their proteic domain rich in serine "S" and arginine "R" (Raj et al, 2011). From literature it is known that the interaction between nSR100 and pre-mRNAs is necessary for exon inclusion and it is mediated by conserved UGC motifs downstream the exon splicing acceptor site regulated by nSR100 (Nakano et al., 2012). A 12 bp sequence UGCUGC it has been identified downstream exon 8a. It is necessary for nSR100 binding and 100% conserved in mammals. Moreover the insertion of only one nucleotide in the consensus sequence of nRS100 (MG800-mut in figure 14) completely abolishes not only the effect of nSR100 on exon 8a inclusion, but also the basal inclusion observed in SH-SY5Y cells, when nSR100 is not overespressed (Fig. 14). This suggested that the basal inclusion of exon 8a in MG ttanscripts is due to the low level of expression of nSR100 observed in SH-SY5Y cells.

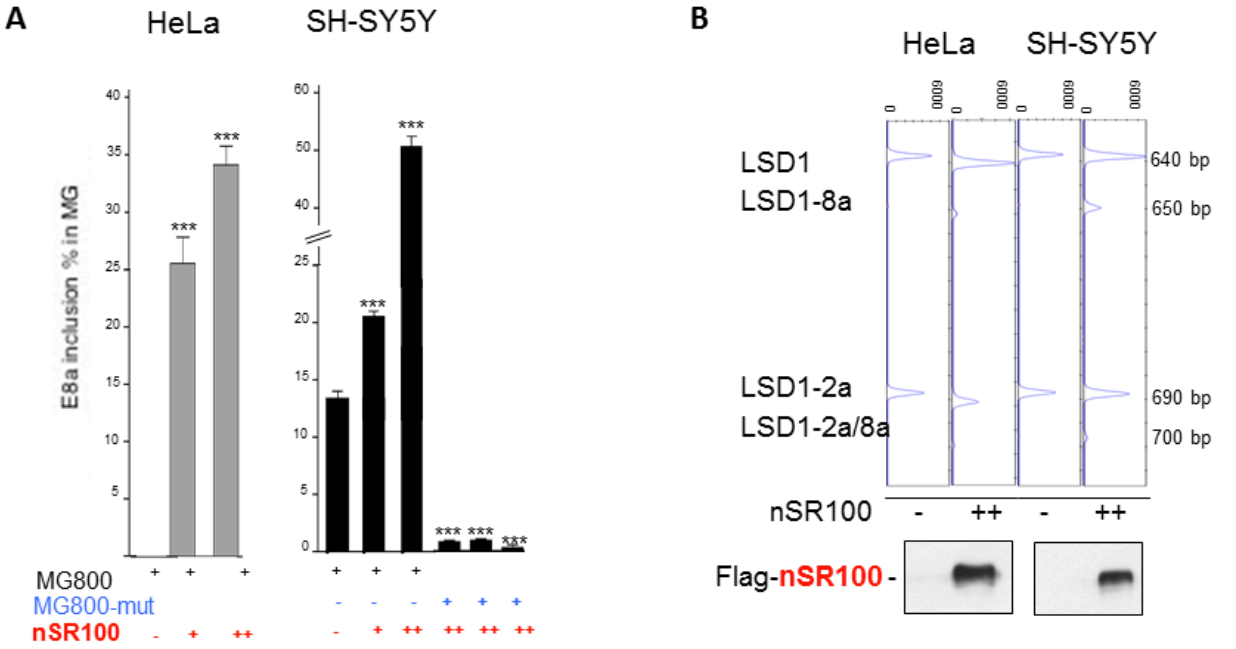

Fig. 14 nSR100 is the principal neurospecific splicing factor responsible of the regulation of the neuroLSD1 expression in neuronal cells. A, nSR100 promots the inclusion of the exon 8a in transcripts derived from minigene hLSD1-MG800 in a dose dependent manner in SH-SY5Y cells; in hLSD1-MG800-Mut exon 8a inclusion is abrogated. B, nSR100 promotes di per se neurospecific splicing in HeLa cells and the level of endogenous LSD1 mRNA in SH-SY5Y. Bars represent error standard, **p≤0,001 Student "t" test. (from Rusconi, 2014)

These results collectively indicate nSR100 as the necessary and sufficient factor regulating LSD1 neurospecific splicing. There are therefore 3 key elements responsible for regulating expression of neuroLSD1 in neuronal cells: a palindromic cis-acting negative regulator and 2 trans-acting neurospecific splicing factors, nSR100 and NOVA1 (Rusconi et al, 2014). NOVA1 and nSR100 cooperate to bind LSD1 pre-mRNAs. Furthermore, performing co-immunoprecipitation experiments using overexpressed HA-NOVA1 and Flag-nSR100, the 2 proteins were found as part of the same splicing regulating complex (Fig. 15). Taken together, these results indicate that nSR100 and NOVA1 and the cis-acting palindrome cooperate in restricting neuroLSD1 expression to the nervous system.

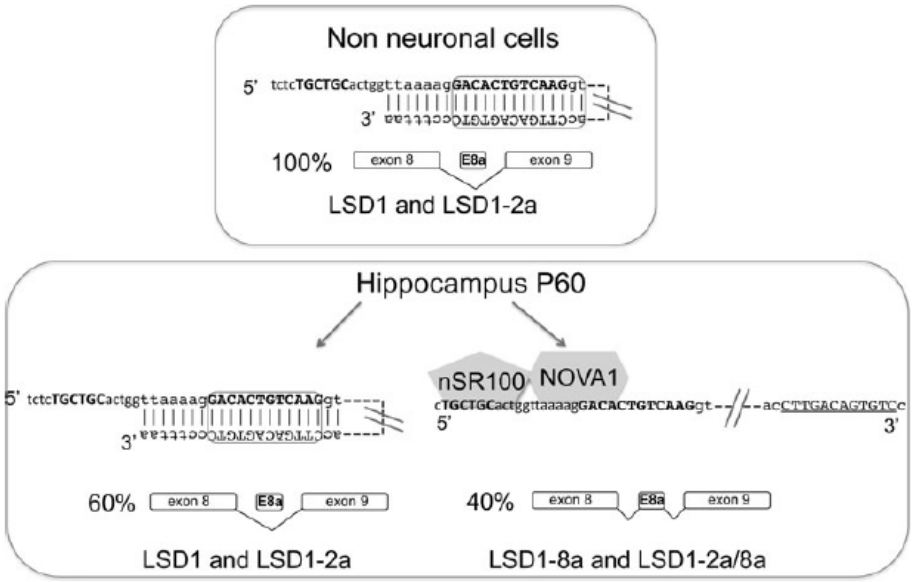

Fig. 15 Schematic model recapitulating exon E8a splicing regulation by cis- and trans-acting factors. In non-neuronal cells where neurospecific splicing factors are absent, exon E8a is never included. In neuronal cells, NOVA1 and nSR100 binding to LSD1 pre-mRNA promote splicing inclusion but have to counteract palindrome annealing to exon E8a in order to expose E8a donor and acceptor splicing sites. In neuronal cells, the presence of the palindrome ensure a fine balance between neuronal and non-neuronal isoforms: for instance, in P60 mouse hippocampus, the ratio between neuronal and non-neuronal isoforms is, respectively, 60% and 40%. In non-neuronal cells, palindrome represents an intrinsic safe lock mechanism to avoid aberrant E8a splicing inclusion

3.3 Generation of neuroLSD1-null mice

The generation in our laboratory of a gene targeting mutant mouse line specifically ablating exon E8a (neuroLSD1^{KO}), was an important tool in order to understand the physiologic relevance of exon E8a in normal and pathological responses in the CNS. The characterization of neuroLSD1KO mice was illustrated in the work of Rusconi et al, 2014. Figure 16 shows that brains lacking neuroLSD1 retain LSD1 expression and display normal morphology. Animals were healthy and did not show any alteration of the vital parameters: weight, dimensions, and fertility were unaffected by the mutation and no morphological defects were detected.

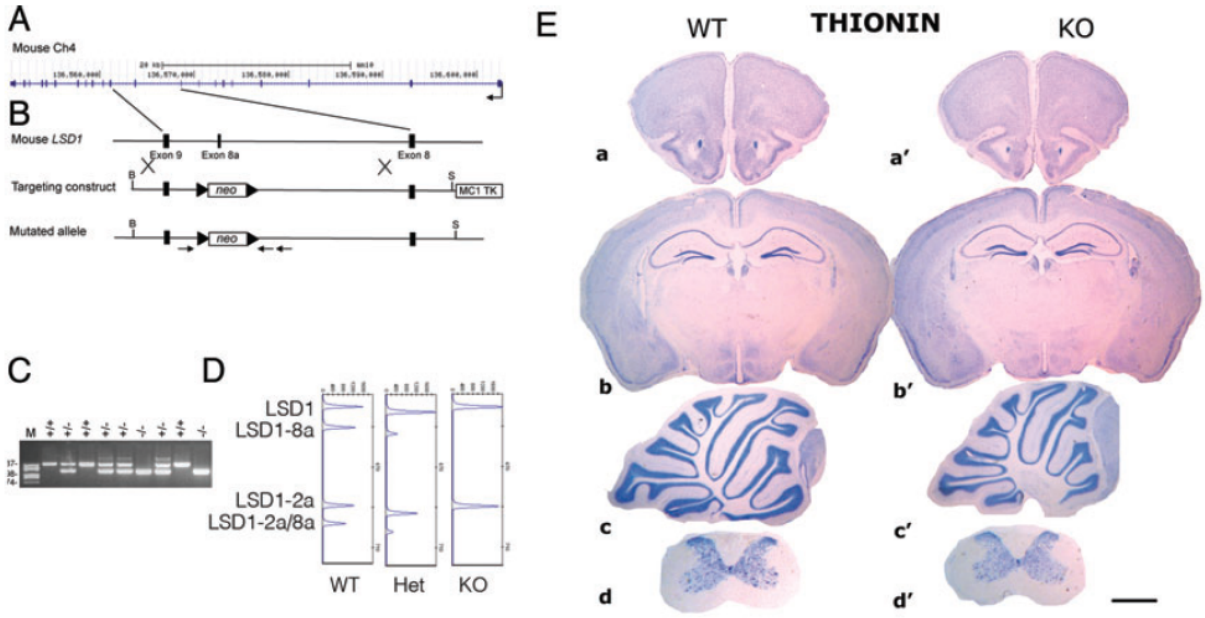

Fig. 16 Brains lacking neuroLSD1 retain LSD1 expression and display normal morphology. (A) Schematic representation of mouse LSD1 gene. (B) Exon E8a deletion strategy: targeting construct and mutated allele are shown. (C) PCR genotyping with primers F1, R1, and R2 on a representative litter of neuroLSD1 +/−. (D) rqfRT-PCR analysis of hippocampal RNA from wild-type, heterozygous, and knockout animals. (E–I) Brain cytoarchitectural analysis of wild-type and knockout adult mice. (E) Photomicrographs of thionin-stained vibratome sections; a, a′, coronal section at the level of frontal cortex and anterior olfactory nuclei; b, b′, coronal section at the level of somatosensory cortex, hippocampus, and diencephalon; c, c′, sagittal section of cerebellum; d, d′, transverse section of spinal cord. Scale bars=1.3 μm for a–b′; 1.9 μm for c–d′.

Immunohistochemistry showed a normal pattern of labeling with anti-GFAP (glial fibrillar acid protein, a marker of astrocytes), indicating absence of astroglial activation (Fig. 17F). Immunohistochemistry showed a normal pattern of labeling with anti- NeuN (neuronal nuclear antigen, a pan-neuronal marker), indicating absence of abnormalities in neuronal distribution and density (Fig. 17G). In the hippocampus, the immunostaining for the calcium binding protein Calretinin was normal (Fig. 17H), whereas a weaker immunostaining for the calcium binding protein Calbindin was evident in the hippocampus dentate gyrus and CA3 of neuroLSD1^{KO} mice compared with wild-type littermates (Fig. 18I). Immunohistochemical localization of LSD1 using a pan-LSD1 antibody showed an identical pattern and intensity of labelling in all brain sections of wild-type and neuroLSD1^{KO} mice analyzed. Finally, also the immunoreactivity for the LSD1 dimethylated substrates H3K4 and H3K9 was unaffected in neuroLSD1^{KO} mice compared with wild-type littermates (Rusconi et al, 2014).

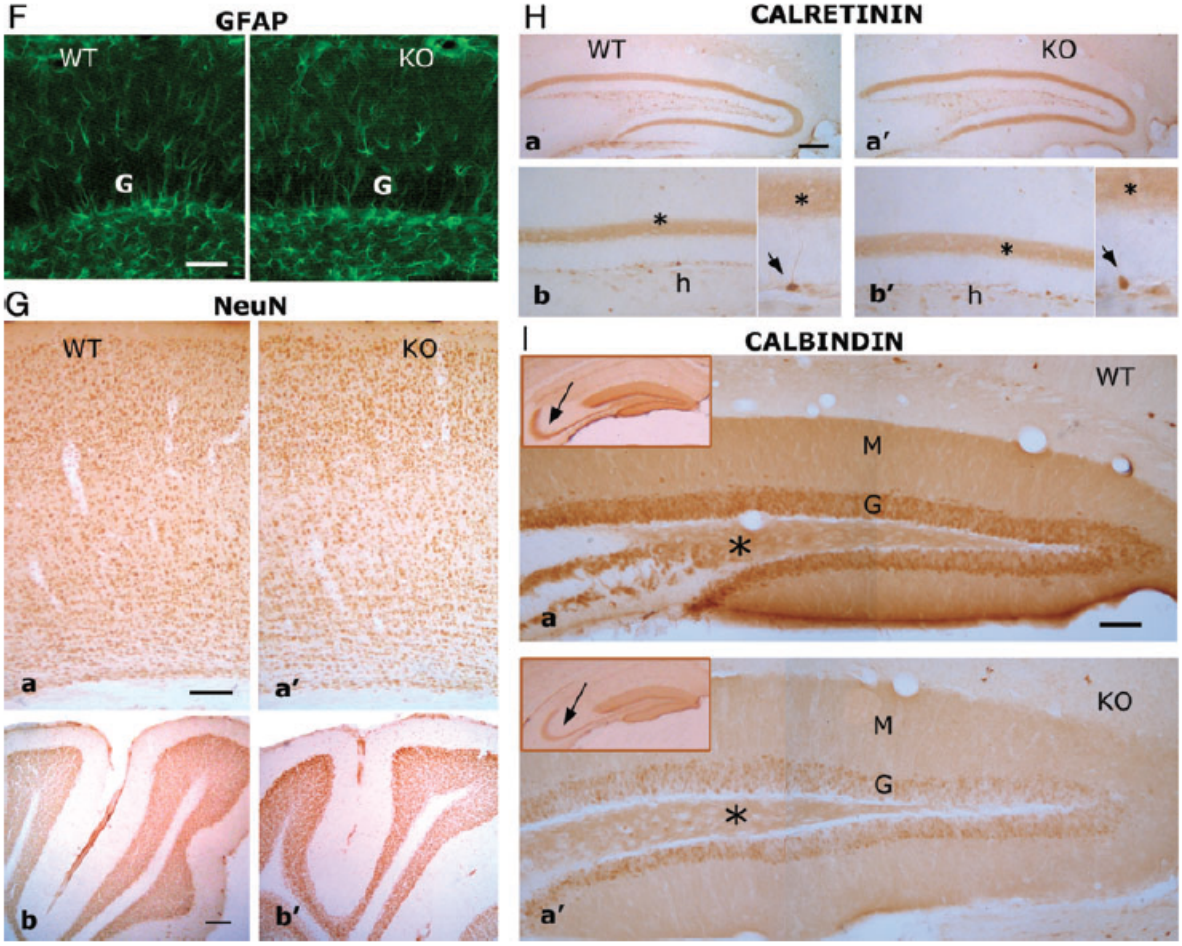

Figure 17. Brains lacking neuroLSD1 retain LSD1 expression and display normal morphology. (F) Immunostaining for GFAP in the hippocampus; G=granule cell layer of dentate gyrus; Scale bar=160 μm. (G) Immunostaining for NeuN in the cerebral cortex a, a′ and cerebellum b, b′. Scale bars=370 μm. (H) Immunostaining for calretinin in the hippocampus; a, a′; b–b′, labeled neurons are in the hilus (h) and subgranular zone (arrowheads) and labeled terminals form a band in the inner molecular layer (asterisks); Scale bars=940 μm for a, a′; 370 μm for b, b. (I) Immunostaining for Calbindin in the hippocampus; a, a′; G=granule cell layer, M=molecular layer of dentate gyrus; asterisks denotes mossy fibers in the hilus. Low power inserts show the mossy fibers projections to the CA3 region (arrows); Scale bars=170 μm, inserts 600 μm.

In the light of these data, the aim of my project was to understand the molecular mechanism at the basis of the different function of neuroLSD1 in the mammalian CNS and to identify new transcription factors that recruit LSD1 to specific gene promoters in the brain in order to regulate transcription of specific target genes.

MATERIALS AND METHODS

Plasmids

Gal4-LSD1 and cGal4-neuroLSD1 containing the full length cDNAs were generated by PCR and cloned into pSG424- vector. The HA-LSD1, HA-neuroLSD1, and the E. coli expression plasmids have been described (Zibetti et al. 2010). Thr369bAla, Thr369bAsp, and Lys661Ala mutants where obtained by site-specific mutagenesis using the QuikChange II Site-Directed Mutagenesis Kits (Stratagene, La Jolla, CA, USA). For lentiviral transduction, HA-fused LSD1 and neuroLSD1Thr369bAsp cDNAs were generated by PCR using pCGN-vectors as templates and cloned into lentiviral transfer vector C-FUW in the AscI and HpaI sites. All plasmids were sequenced.

Animals

Animals were obtained from Charles River, Calco, Italy. All the animal treatments followed the guidelines established by the Italian Council on Animal Care and were approved by the Italian Government decree No. 27/2010 being in compliance with the ARRIVE guidelines. All efforts were made to minimize the number of subjects used and their suffering. Immunopurification of LSD1 from brain extract and in situ digestion and mass spectrometry. Total protein extracts were obtained from post-natal day 1 rat brains (Charles River) lysed in immunoprecipitation (IP) buffer (10% glycerol, 0.5 mM EDTA, 0.5% Triton-X100, 1 mM phenylmethylsulfonyl fluoride), and 19 Protease Inhibitors Cocktail, (Sigma-Aldrich, St. Louis, MO, USA). Two milligram of cellular extract were reacted with 2.5 lg of rabbit polyclonal anti-LSD1 antibody (AbCam, Cambridge, UK) overnight rocking at 4°C. The immunoprecipitates were collected with Protein G Agarose (Invitrogen, Carlsbad, CA, USA). After incubation, the beads were washed four times with the IP buffer. The immunoprecipitates were then eluted with 1x sodium dodecyl sulfate Sample buffer and separated on 1D polyacrylamide. Following mass compatible silver staining, the protein band at 110 KDa band corresponding to the LSD1 molecular weight excised, destained with 50% acetonitrile in ammonium bicarbonate 0.1 M (40 min at 25°C), dried in a Speed Vac, soaked with ammonium bicarbonate 0.1 M, reduced and derivatized by iodoacetamide, and digested overnight with trypsin sequencing grade (Roche, Monza, Italy) at 37°C (Pastori et al. 2010). The in gel tryptic digest was extracted with 50% acetonitrile in 0.1% trifluoroacetic acid. Digested aliquots were removed and subjected to a desalting/concentration step on a lZipTipC18 (Millipore, Bedford, MA, USA) using 40% CH3CN in 0.1% trifluoroacetic acid as eluent before MALDI analysis usingan Autoflex III instrument (Bruker Daltonics,

Bremen, Germany). For protein identification, the Biotools software (Bruker Daltonics, Milano, Italy) was used to search the NCBI protein Data Bank by setting carbamidomethylation as fixed modification and by setting oxidation (M), phosphorylation (Ser, Thr and Tyr), and deamidation (Asn and Gln) as variable modifications. Two missed cleavages were allowed. Peptide quality scores were derived by processing against decoy shuffled databases.

Stable cell lines

HA-tagged human LSD1 or neuroLSD1 cDNAs (Zibetti et al. 2010) or neuroLSD1-Thr369bAsp or neuroLSD1-Thr369bAla were transfected into HeLa cells together with pPURO (Clontech Takara-Bio, Mountain View, CA, USA). Stable clones were selected against Puromycine (0.5 lg/mL) and screen for HA expression.

Immunoprecipitation and HDAC activity assay

Immunoprecipitation experiments were performed as previously reported (Battaglioli et al. 2002). HeLa cells or cortical neurons were harvested in IP buffer (10% glycerol NaCl 150 mM, imidazole 10 mM, 0.5 mM EDTA 0.5% Triton-X100, dithiothreitol 0.5 mM) supplemented with 1 mM phenylmethylsulfonyl fluoride and 1x Protease Inhibitors Cocktail and 1x Phosphatase Inhibitor Cocktail (Roche). 0.5 mg of cellular extract were reacted and collected with HA-conjugated Agarose beads (Santa Cruz, Santa Cruz, CA, USA). After incubation, the beads were washed four times with IP buffer. The immunoprecipitates were then eluted with 1x sodium dodecyl sulfate Sample buffer and analyzed using western Blot. Quantification was performed using ImageJ software (ImageJ 1.43u National Institute of Health, Washington, DC, USA). Immunoprecipitates with 5 lg of the monoclonal anti-HA antibody (Santa Cruz) obtained from 2 mg of total cell extracts were tested for their histone deacetylate activity (Active Motif, Carlsbad, CA, USA). Immunoprecipitates collected using Dynabeads (Invitrogen) were incubated for 60 min with a short peptide substrate containing an acetylated lysine residue that can be deacetylated by Class I, II, and IV HDAC enzymes. Once the substrate is deacetylated, the lysine reacts with the developing solution and releases a fluorescent product measured using a fluorescent plate reader with an excitation wavelength of 340–60 nm and emission wavelength of 440–465 nm. We performed developing reaction for 10 min. Histone deacetylase activity was normalized for immunoprecipitation efficiency on western blot using an anti-HA antibody and expressed as fold over the mock condition. The reaction was read using a microplate reader

Wallac 1420 VICTOR3 V (Perkin Elmer, Waltham, MA, USA).

Lentiviral infections

HA-LSD1 and Ha-neuroLSD1-T369bD were subcloned into the lentiviral transfer vector FUW which contains the ubiquitin promoter (Lois et al. 2002). The preparation of the lentivirus vectors has been previously described (Naldini et al. 1996; Lois et al. 2002). Neurons were infected after 4 days in vitro (DIV4) and analyzed on DIV8.

Total RNA extraction and RT-PCR analysis

Total RNA was isolated using the Trizol reagent (Sigma- Aldrich), and the purified RNA was treated with RNase-free DNase set (Qiagen, Valencia, CA, USA) to remove any residual DNA. Quantitative RT-PCR analysis was performed on an iQ5 Real-Time PCR Detection System (Biorad, Hercules, CA, USA) using the iScriptTM two-Step RT-PCR Kit with SYBR_ Green (Biorad). The relative expression of the investigated genes was quantified after normalization against ribosomal protein SA (RPSA) and glyceraldehyde-3- phosphate dehydrogenase (GAPDH). RT-PCR was performed with BioTaq DNA Polymerase (Boline, London, UK).

Primers

Cloning primers:

cFUW-LSD1 Fw GCGTTAAGCGGACCATGGCTTCTAGCCTATCCTTA

cFUW-LSD1 Rv CCGGGCGCGCCTCACATGCTTGGGGACTGCTGTGC

hLSD1-Thr/Asp Fw CAAGCTGACGATGTCAAGGTTCCT

hLSD1-Thr/Asp Rv AGGAACCTTGACAGCGTCAGCTTG

hLSD1-Thr/Ala Fw CAAGCTGACGCTGTTCAAGGTTCCT

hLSD1-Thr/Ala Rv AGGAACCTTGACAGCGTCAGCTTG

Primers for splicing quantification

Human-LSD1 Fw GTGAGCCTGAAGAACCATCG (E2) or

Fw GAAAAGGAAACTATGTAGC (E8)

Human-LSD1 Rv CTACCATTTCATCTTTCTCTTTAGG

Mouse-LSD1 Fw AGTGAGCCGGAAGAGCCGTCTG (E2) or

Fw GAAAAGGAAACTATGTAGC (E8)

Mouse-LSD1 Rv CTACCATTTCATCTTTTTCTTTTGG

Primers for mice genotyping

P3 Fw ACGCGTCGACTCTTCAGTGCTTTCTCACTCCCA

P6 Rv ATAGTTTAGCGGCCGCCCTCTATTTTCTGAGCAGCC

PB Rv CAGCTGGGGCTCGACTAGAGCTTGC

Primers for semiquantitative RT-PCR

Actine Fw ACC TGG CCG TCA GGC AGC TC

Actine Rv CCG AGC GTG GCT ACA GCT TC

Primers for RealTime qPCR (rat)

mRPSA Fw ACCCAGAGGAGATTGAGAAGG

mRPSA Rv TGGGGAACTGCTGGATGGGC

GAPDH Fw GGAAACCCATCACCATCTTCC

GAPDH Rv GAAGGGGCGGAGATGATGACC

CK5R1 Fw AGCCCTTCCTGGTGGAGAG

CK5R1 Rv AAGTCAGAGAACACTTGTGTG

EGR1 Fw TTCAATCCTCAAGGGGAGC

EGR1 Rv AACCGGGTAGTTTGGCTGGGA

c-FOS Fw CTGCAGCCAAGTGCCGGAAT

c-FOS Rv TTGGCAATCTCGGTCTGCAAC

PCTAIRE Fw TCGTGTTCCAGTCTGATCTCC

PCTAIRE Rv TCGTGTTCCAGTCTGATCTCC

GRIN1 Fw GGTGGCTGTGATGCTGTAC

GRIN1 Rv TCCTCCTCCTCACTGTTCAC

PSD95 Fw CAAGATCCTGGCGGTCAAC

PSD95 Rv CGTCATATGTGTTCTTCAGGG

Primers for ChIP analysis (mouse)

c-FOS Fw TCAGAGTTGGCTGCAGCCGGC

c-FOS Rv GCGTGTAGGATTTCGGAGATG

Cdkl4 Fw ACCACAGAACTCCCGAGAGACC
Cdkl4 Rev GGTGATGGATGGAAGGTAACC
EGR1-CTRL- Fw GGCCTGGGTCACAGACCTAC
EGR1-CTRL- Rv CTTCTGTGTACCCAGCACCTG
Egr1 Fw GGCCTGGGTCACAGACCTAC
Egr1 Rv CTTCTGTGTACCCAGCACCTG

Cortical neuron cultures and immunostaining

Cortical neuron cultures were prepared from embryonic day 18 (E18–E19) rat brain (Charles River) as previously described (Romorini et al. 2004), plated on 18 mm diameter cover slips, and grown on 12-well plastic tissue culture plates (Iwaki; Bibby Sterilin, Staffordshire, UK). The neurons were transfected using calcium phosphate precipitation (transfection efficiency 1%). Cells were fixed with a phosphate- buffered saline solution containing 4% paraformaldehyde for 10 min. Cells were incubated anti-HA (1 : 100 sc80; Santa Cruz) for 3 h at 23°C in gelatin dilution buffer (30 mM phosphate buffer, pH 7.4, containing 0.2% gelatin, 0.5% Triton X-100, and 0.8 M NaCl), followed by FITC-conjugated secondary antibodies (Jackson Laboratories, Bar Harbor, ME, USA) for 1 h. The images were acquired using a Zeiss LSM5 510 laser-scanning confocal microscope (Oberkochen, Germany, generously donated by Fondazione Monzino) at 63x magnification, and an Axioplan fluorescent microscope at 259 magnification.

Spine analysis

Labelled transfected neurons were chosen randomly for quantification from four coverslips from three independent experiments for each construct. Fluorescent images were acquired with a Zeiss 510 confocal microscope, using a 60X objective with sequential acquisition setting at 1,240 X 1,240 pixel resolution. Image data were a z series projection of about 5–8 images, each averaged 4 times and taken at 0.7 μm depth intervals. Morphometric measurements were made with NeuronStudio software. All measurements are given as mean standard error of the mean (s.e.m.).

Reporter gene assays

Cortical neurons were cultured and transfected at DIV4 using calcium phosphate precipitation. 5xUAS-TK-LUC reporter plasmid (Chen et al. 1998) was used at the indicated molar ratio relative to the expression plasmids pGal4-LSD1, pGal4- neuroLSD1, and mutants. Control

experiments were carried out by using equivalent molar amounts of pGal4 empty vectors. DNA was kept constant by adding pBSIIKS (Stratagene) in every experiment; pRL-TK-vector (Promega, Madison, MI, USA) reporter vector was co-transfected to normalize for transfection efficiency. The luciferase reporter activity was determined with the Dual-Luciferase reporter assay system (Promega) according to the manufacturer's instructions. For each construct, the values of Firefly luciferase were normalized over Renilla luciferase (both expressed as relative luminescent units). The activity of each construct was expressed as a percentage of the promoter-less plasmid pGal4-vector.

Biochemical assays and structural analysis of theThr369bAsp phospho-mimetic mutant

Recombinant neuroLSD1/CoREST proteins were expressed in E. coli and purified following the same protocols used for the expression and purification of wild-type LSD1/CoREST (Zibetti et al. 2010). Likewise, the enzymatic activities were measured as described (Forneris et al. 2007). Crystals of Thr369bAsp LSD1/CoREST were grown at 20°C by hanging- drop vapor diffusion method by mixing equal volumes of protein samples with reservoir solutions containing 1.2 M sodium/potassium tartrate and 100 mM N-(2-acetamido) iminodiacetic acid, pH 6.5 (Forneris et al. 2007). Crystals were flash cooled in liquid nitrogen and data collections were performed at the beam-lines of the European Synchrotron Radiation Facility and of the Swiss Light Source. Data processing and crystallographic refinements were performed using programs of the CCP4 package (Winn et al. 2011). The crystallographic statistics are the following: resolution, 3.1 _A; number of unique reflections, 44180; Rmerge, 0.102 (0.601 in the highest resolution shell); multiplicity 4.5 (4.1); Rfactor and Rfree of the refined model, 0.209 and 0.226; root-mean-square deviation for bond-lengths and bondangles, 0.005 _A and 0.91°.

Chromatin immunoprecipitation

Hippocampi of 8 weeks old mice have been dissected and rapidly incubated in 1% formaldehyde for 15 minutes at RT for cross-linking purposes then transferred in 0.125 M glycine for 10 minutes and homogenized in lysis buffer (10 mM Tris- HCl pH 8; 1 mM EDTA, 0.5 mM EGTA, 100 mM NaCl, 0.1 % Na-deoxy-cholate, 0.5% N-laurylsarcosine) containing protease inhibitors and PMSF 0.2 mM. Lysates were sonicated twice with a Bandeline Electronic Sonicator for 30 seconds at 30% power to generate fragments with an average length of ~500-200 bp, as determined empirically by agarose gel electrophoresis of the fragmented chromatin sample.

Immunoprecipitation was performed overnight with 200 µl of sonicated chromatin in 600 µl of lysis buffer containing Triton 1%, PMSF 0.2 mM and 1.2 µg of anti-MeCP2 pAb (SIGMA, Saint Louis, USA). A sample without antibody (mock) was included as a control. The samples were then incubated with protein G Dynabeads (Invitrogen Corporation, Carlsbad, CA) at 4°C for 2 hours. After immunoprecipitation, the mock supernatant was kept apart as input sample. The beads were washed sequentially at 4°C (for 7 minutes each) with 800 µl of low salt buffer (0.1% SDS, 2mM EDTA, 1% Triton, 20mM Tris-HCl pH 8, 150 mM NaCl), high salt buffer (0.1% SDS, 2mM EDTA, 1% Triton, 20mM Tris-HCl pH 8, 500 mM NaCl and TE buffer (10 mM Tris-HCl pH 8, 1 mM EDTA pH 8.0), then again with low salt buffer and with high salt buffer. At the end the beads were washed with TE-NaCl buffer (10 mMTris-HCl, 1 mM EDTA, 50 mM NaCl). Elution was performed in 100µl of fresh elution buffer (1% SDS, 0.1 M NaHCO3). Cross-linking was reversed overnight at 65°C. After cross-link reversal, 240 µg of Ribonuclase A (SIGMA, Saint Louis, USA) were added to each samples to completely eliminate the RNA and the samples were incubated for 40 minutes at 37°C.

The samples were then digested with 20 µg of proteinase K (SIGMA, Saint Louis, USA) for 1 hour at 56°C, and DNA was recovered by standard methods in 20 µl of 10 mM Tris-HCl pH 8. Promoters were analyzed by quantitative real-time PCR using 1 µl of each immunoprecipitated samples and 1 µl of the input 1:100 dilution. Real time PCR was carried out using iTaq Universal SyberGreen Supermix (Biorad) with a iQ5 (Biorad) according to manufacturer's instructions. The primers used in the PCR real-time reaction are listed in the primers section. ChIP experiment data result from at least three independent experiments, and all quantitative real-time PCR experiments were performed in duplicate. Relative proportions of immunoprecipitated DNA were determined based on the threshold cycle (Ct) value for each PCR reaction. In order to control for variation between ChIP fractions, for every gene promoter studied, a ΔCt value was calculated for each sample by subtracting the Ct value for the input (Ct Input) from the Ct value for the immunoprecipitated sample (Ct antibody or Ct mock). Because the input DNA fraction represents only 1% of the total material, the Ct Input value was first adjusted for this dilution factor by subtracting 6.644 cycles (Log2 of 100). Data were then plotted as fold enrichment over mock.

RESULTS

1 PHYSIOLOGICAL RELEVANCE OF LSD1/neuroLSD1 SPLICING RATIO IN NEURONS

1.1 Exon E8a coded Thr369b can be phosphorylated in the brain

Three-dimensional crystal structure analysis of recombinant LSD1/CoREST proteins indicated that the four additional amino acids of exon E8a form a loop protruding out of the protein surface on the rim of the active site cleft. Importantly, such a loop appeared to be fully accessible for possible post-translational modifications (PTM) (Zibetti et al. 2010). For consistency with the previous publications and with numbering scheme used for the coordinates deposited with the Protein Data Bank, we shall number the four residues of the exon E8a, inserted between Ala369 and Val370, as Asp369a- Thr369b-Val369c-Lys369d. We scanned the 856 amino acid long neuroLSD1 variant using NetPhos v2.0 software (http:// www.cbs.dtu.dk/services/NetPhos) to identify putative phosphorylation sites. Thr369b coded by exon E8a was predicted as a high-score potential site of phosphorylation (Fig. 19a). In order to verify this prediction, rat brain tissues collected at P1, when neuronal neuroLSD1 protein is highly expressed, were used to immuno-isolate LSD1 complexes with a pan- LSD1 antibody. Immunocomplexes were separated by sodium dodecyl sulfate–polyacrylamide gel electrophoresis, and the 110 KDa band corresponding to LSD1 was processed for mass spectrometry. The analysis indicated the presence of LSD1 peptides containing phosphorylated and non-phosphorylated exon E8a (Fig. 19b and c). Moreover, Tyr363 was also phosphorylated, in line with its very high predicted phosphorylation score (Fig. 19a and b).

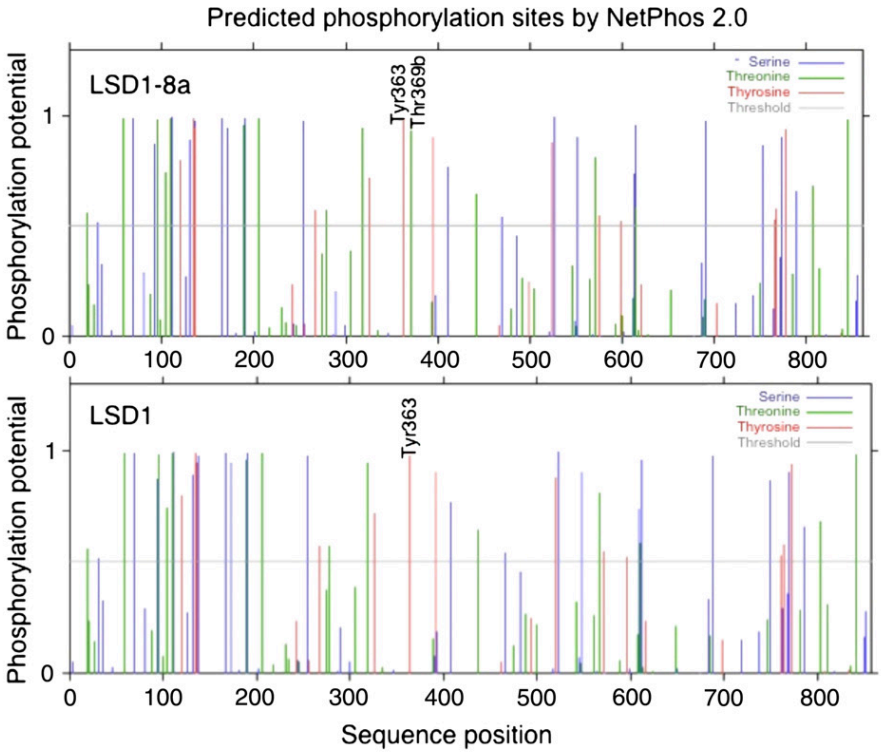

LSD1 peptides identified in rat brain containing phosphorylated and non-phosphorylated Thr369b

Peptide	Species	Calculated MW	Observed MW
$_{360}$CPLYEANGQA**DTVK**$_{369b}$	Cys_CAM	1565.73	1566.04
$_{360}$CPLYEANGQA**DTVK**$_{369b}$	Cys_CAM, 2P (+160)	1725.73	1725.10
$_{360}$CPLYEANGQA**DTVK**VPK$_{372}$	Cys_CAM, 1P (-18)	1871.94	1871.60
$_{356}$IKQKCPLYEANGQA**DTVK**$_{369b}$	Cys_CAM, 1P (-18)	2045.06	2044.06

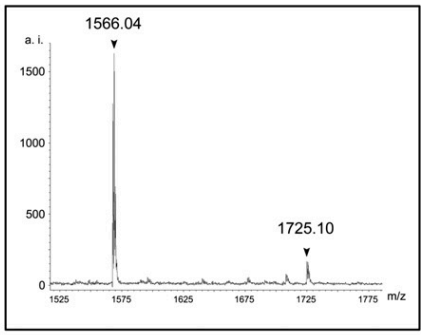

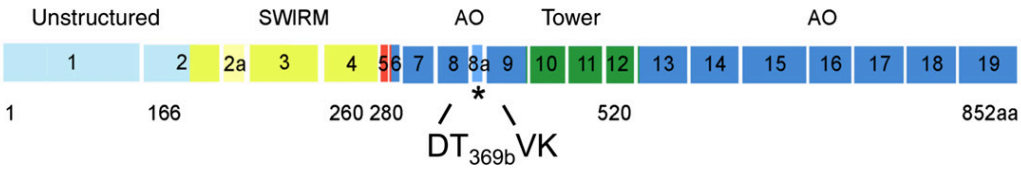

Fig 19 Lysine-Specific Demethylase 1 (LSD1)-8a Thr369b coded by exon E8a can be phosphorylated in the brain. (a) Probability plot of phosphorylation sites was computed on NetPhos v.2.0 software spanning through the 856 amino-acid long NeuroLSD1 compared to conventional LSD1. (b) Mass spectrometry analysis of LSD1 immunopurified from post-natal day 1 rat brain revealed peptides containing phosphorylated and non-phosphorylated exon E8a. The presence of one phosphate group leads to an increase in mass of 80 units (Thr,Ser,Tyr) or a decrease of 18 units because of the loss of the phosphate and a water molecule (Thr, Ser). The molecular weights are given as monoisotopic mass. Cys_CAM indicates the presence of a carbamidomethylated Cys residue because of the derivatization of the protein by iodoacetamide as described in Methods. (c) Spectrum of the peptide 360–369 in phosphorylated (1725.10) and non-phosphorylated (1566.04) state. (d) Thr369b position is indicated relatively to exons and functional domains in hLSD1.

1.2 Phosphorylation of Thr369b induces CoREST, HDAC1, and HDAC2 disassembly

1.2.1 Generation of Hela cells stably expressing HA-tagged LSD1 isoforms and mutants

To study the effect of Thr369b phosphorylation on protein activity, we decided to generate two different mutants of neuroLSD1, the first called neuroLSD1-Thr369bAsp (T/D), carrying Threonine 369b substitution with Aspartate (Thr369bAsp) and costituting the phospho-mimetic form, and the second called neuroLSD1-T369bA (T/A), carrying Threonine 369b substitution with Alanine, and costituting the phospho-defective mutant.

Proteic phosphorylation is a simple and reversible post-tradutional modification, that controls a large amount of cellular processes. It is a covalent modification that entails the transfer of the γ -phospate of a donor molecule as ATP or GTP to alcholic or phenolic aminoacidic residues. Phospho group introduces in the protein a negative charge with a large steric obstruction. This causes a riorganization of the bindings in the ternary stucture of the protein. As shown in figure 20, threonine residue has a OH group that can be phosphorilated, the aspartate residue has a negative charge that mimics the phosphorylation, while the lateral chian of the Alanine residue is characterized by a non-nucleophile, methylic group that cannot be phosphorylated.

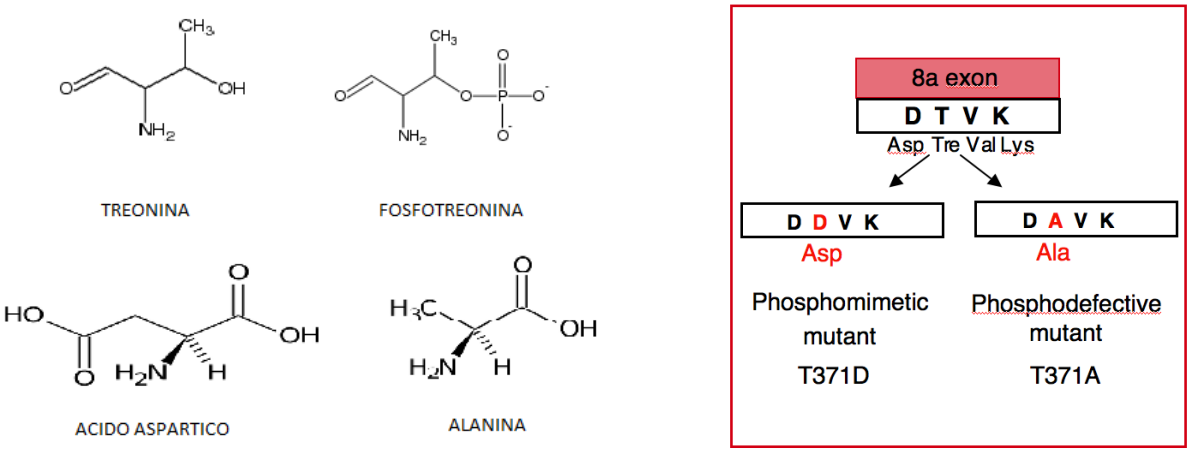

Fig 20 Structural formula of the four aminoacids threonine, phosphothreonine, aspartic acid and alanine and scheme of the mutations of threonine T369bD and T369bA

To study the effects of these mutants we chose to stably transfect them in Hela cells. We chose to generate HeLa cells mainly because of the experimental manipulability of the cell type when performing biochemical studies. We produce Hela cells stably expressing LSD1, neuroLSD1, neuroLSD1T/D and neuroLSD1-T/A. Figure 21B shows the experimental plan of the generation of the clones stably expressing mutant proteins. This proteins are fused with HA epitope to allow protein immunoprecipitation and further experiments.

To generate stable cells, the plasmids of interest are cotransfected with the pPUR plasmid, carrying the puromycine resistance. Clones able to survive in puromycine selective medium, are then screen for HA expression. We finally chose clones expressing similar level of protein. Figure 22 shows the HA screening for Hela expressing LSD1 and neuroLSD1 but the same strategy was used to generate and choose TD and TA clones.

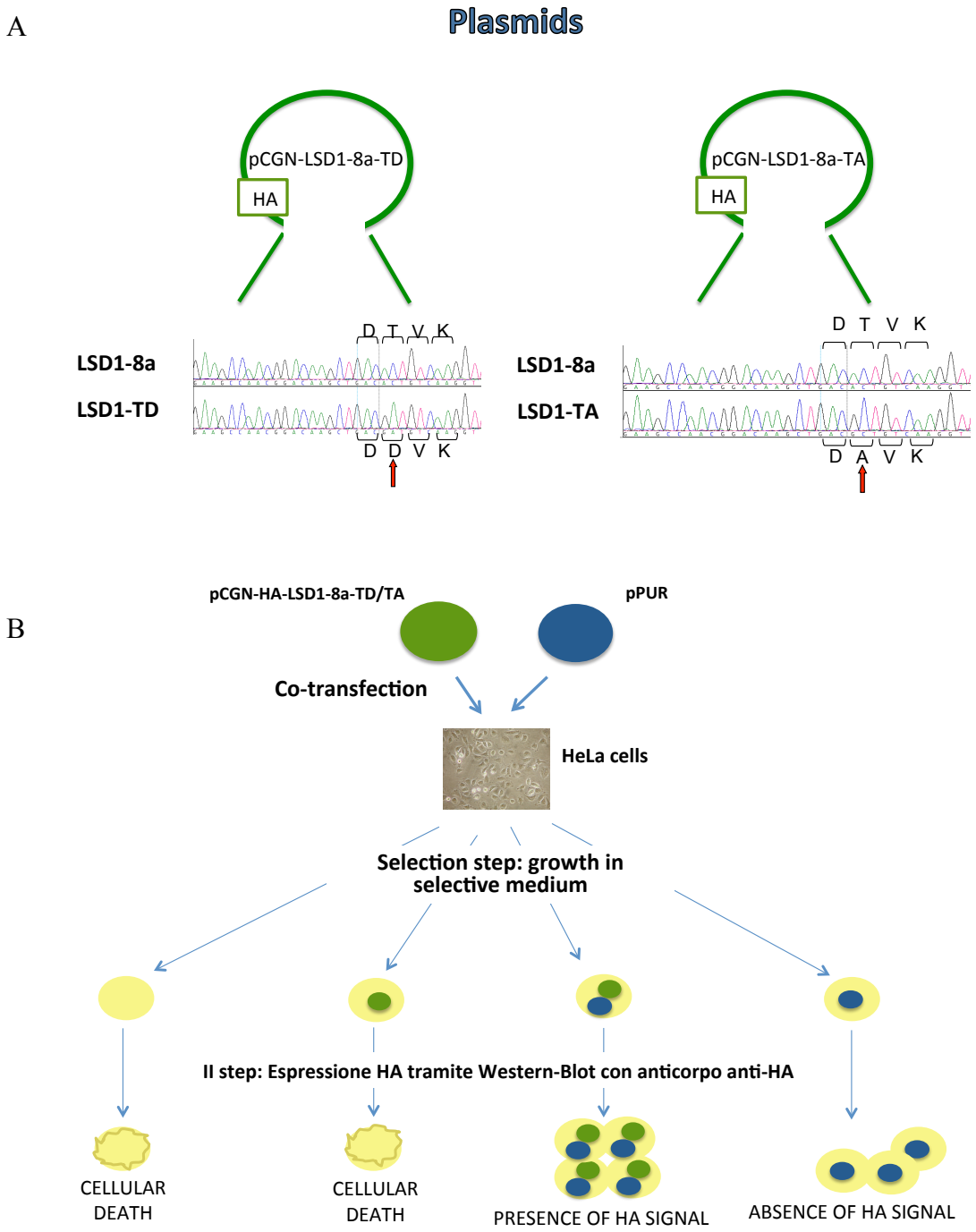

Fig 21 generation of HeLa cell lines stably expressing different HA-tagged LSD1 splicing varants. a) Schematic representation of pCGN plasmids containing Thr/Asp and Thr/Ala LSD1 mutants. Electropherograms of the mutated sequences are shown. b) Experimental plan of HeLa cells stable tranfection with pCGN-neuroLSD1-TD or pCGN-neuroLSD1-TA and screening using western blot. Cells integrating no plasmids or only LSD1 containing plasmids, are not able to survive after first selection step in puromycine. Cells integrating in their own genome pPUR plasmid carrying the puromycine gene can survive and are submitted to the second screening step, the expression analysis for HA using anti-HA antibody.

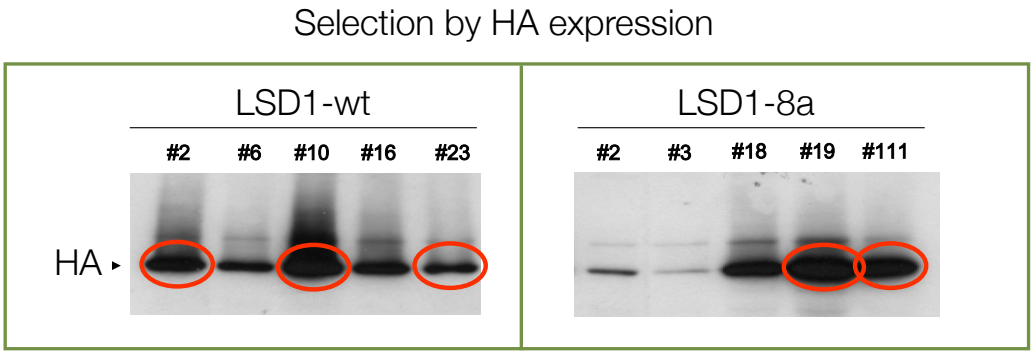

Fig 22 Expression analysis of stably transfected Hela clones

1.2.2 Coimmunoprecipitation analysis

Using anti-HA conjugated agarose beads, we isolated LSD1 complexes in protein extracts obtained from HeLa clones, each stably expressing HA-LSD1, HA-neuroLSD1 and mutants. As mock condition, we used HeLa clones stably expressing the HA-tag from the pCGN empty vector. To test whether the structural alteration induced by the phospho-mimetic mutation affects its ability to recruit CoREST, HDAC1 and HDAC2, we performed immunoprecipitation assays using HeLa cells expressing HA-tagged LSD1, neuroLSD1, or the phosphomimetic NeuroLSD1-Thr369bAsp as well as phospho-defective NeuroLSD1-Thr369bAla mutants.

In accordance with previously published data (Zibetti et al. 2010), LSD1 and neuroLSD1 immunocomplexes were found to contain similar amounts of CoREST, HDAC1, and HDAC2 (Fig. 23a, b; LSD1 vs. NeuroLSD1: CoREST 1 ± 0.23 vs. 0.68 ± 0.16; HDAC1 1 ± 0.08 vs. 0.81 ± 0.03; HDAC2 1 ± 0.04 vs. 1.08 ± 0.04). Remarkably, the immunocomplexes isolated by the phospho-mimetic neuroLSD1-Thr369bAsp mutant showed almost complete lack of the three co-repressors when compared to either NeuroLSD1 or LSD1 (Fig. 23a, b; neuroLSD1-Thr369bAsp vs. neuroLSD1: CoREST 0.17 ± 0.04 vs. 0.68 ± 0.16; HDAC1 0.11 ± 0.01 vs. 0.81 ± 0.03; HDAC2 0.25 ± 0.1 vs. 1.08 ± 0.04, $p < 0.05$; NeuroLSD1- Thr369bAsp vs. LSD1: CoREST 0.17 ± 0.04 vs. 1 ± 0.23, $p < 0.01$; HDAC1 0.11 ± 0.01 vs. 1 ± 0.08, $p < 0.05$; HDAC2 0.25 ± 0.1 vs. 1 ± 0.04; $p < 0.05$). Conversely, the phospho-defective mutant neuroLSD1-Thr369bAla did not show differential association with corepressors, compared to neuroLSD1 (Fig. 23a, b; neuroLSD1-Thr369bAla vs. neuroLSD1: CoREST 0.71 ± 0.09 vs. 0.68 ± 0.16; HDAC1 0.82 ± 0.003 vs. 0.81 ± 0.03; HDAC2 0.85 ± 0.003 vs. 1.08 ± 0.04). These quantifications derived from at least three independent experiments with two independent HeLa clones for each isoform or mutant. To confirm that phosphomimetic NeuroLSD1-Thr369bAsp mutant is unable to assemble CoREST/HDAC1/2 corepressor complex, we used anti-HA conjugated agarose beads to isolate

LSD1 complexes from protein extracts obtained from primary cortical neurons, virally transduced with HA-tagged LSD1, or the phosphomimetic neuroLSD1-Thr369bAsp mutant. As for HeLa cells, we found that also neuronal neuroLSD1-Thr366bAsp immunocomplexes contained largely reduced amounts of Co-REST, and HDAC2 (Fig. 23c).

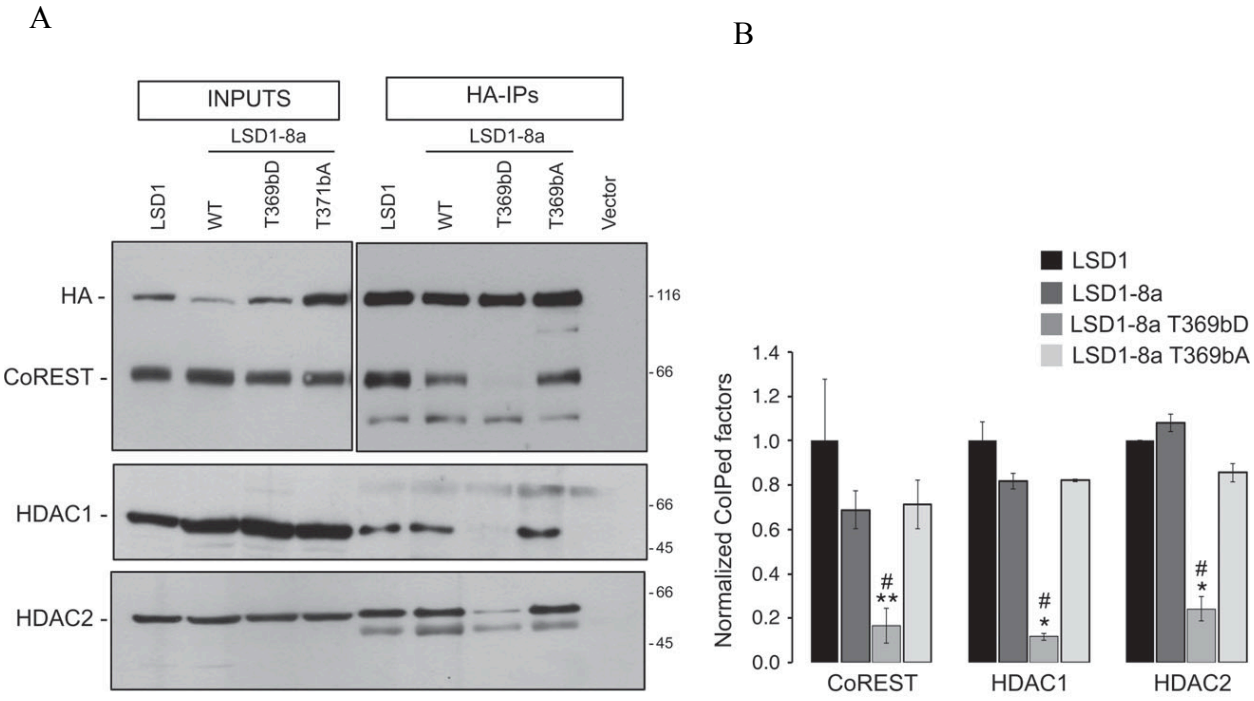

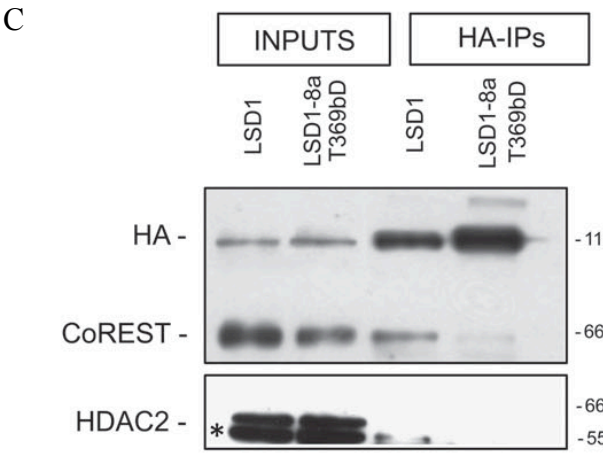

Fig 23 Phosphorylation of Thr369b induces CoREST, HDAC1 and HDAC2 detachment from neuroLSD1 (a) HA-immunocomplexes from HeLa clones stably expressing, HA-LSD1, HA-neuroLSD1, HA-neuroLSD1-Thr369bAsp, and HA-neuroLSD1-Thr369bAla, probed with the indicated antibodies. (b) Quantification of co-immunoprecipitated factors normalized for immunoprecipitation efficiency, expressed as ratio of LSD1. Mean values SEM. Statistical analysis revealed significant differences (*p < 0.05, **p < 0.01 vs. LSD1; #p < 0.05 vs. NeuroLSD1). (c) HA-immunocomplexes from rat cortical neurons virally transduced with HA-LSD1 or HA-NeuroLSD1-Thr369bAsp, probed with the indicated antibodies. The asterisk indicates the 55 KDa band of HDAC2. The slower migrating is a non-specific band. Mean values ± SEM. Statistical analysis revealed significant differences (**p < 0.01 vs. Vector; #p < 0.05 vs. NeuroLSD1). Kruskal Wallis one-way ANOVA followed by Dunn's post hoc test.

1.2.3 Phosphorylation of Thr369b reduces associated deacetylase activity

Given the possibility that other deacetylases might still be present in the neuroLSD1-Thr369bAsp complex or might be de novo recruited, we measured residual deacetylase activity in HeLa cells. We use a fluorescent HDAC Assay kit (Active Motif), an easy and sensitive assay that utilizes a short peptide as substrate that contains an acetylated lysine residue that can be deacetylated by Class I, II e IV HDAC enzymes. Once the substrate is deacetylated, the lysine residue reacts with the developing solution and releases the fluorophore from the substrate resulting in a fluorescent product that can be easely measured using a fluorescent plate reader with an excitation wavelenght of 340-360 nm and emission wavelenght of 440-465 nm. We started from 2mg of proteins from Hela cells stably expressing LSD1, neuroLSD1, neuroLSD1T369bD and from Hela cells stably transfected with the pCGN-HA vector (mock condition), and we immunoprecipitated them with anti-HA antibody. Using anti-HA conjugated agarose beads, we isolated LSD1 complexes and we tested the HDAC activity associated.

We found that residual enzymatic activity bound to HA-neuroLSD1-TD was comparable to the mock condition and reduced compared to LSD1 and neuroLSD1 (Fig. 24; Mock vs. LSD1 1 vs. 15.3 ± 3.5; $p < 0.01$; Mock vs. NeuroLSD1 1 vs. 7.8 ± 1.5; Mock vs. neuroLSD1T/D: 1 vs. 1.9 ± 0.5, $p < 0.05$). Note that the difference in HDAC activity associated to neuroLSD1 showed a tendency towards reduction compared to LSD1. We cannot exclude that, at least in part, overexpressed neuroLSD1 could be phosphorylated in HeLa cells being responsible for partial loss of HDAC activity.

These results strongly suggest that the presence of the phospho-mimetic mutation renders NeuroLSD1 unable to recruit any deacetylase activity. In this regard, it should be noticed that a short fragment of human CoREST (residues 308–440) is able to bind in vitro the phospho-mimetic LSD1-8a mutant (Fig. 19) indicating either that full-length CoREST is required to be disassembled, or that in the cellular context, an additional factor is recruited by the phosphorylated loop leading to CoREST displacement.

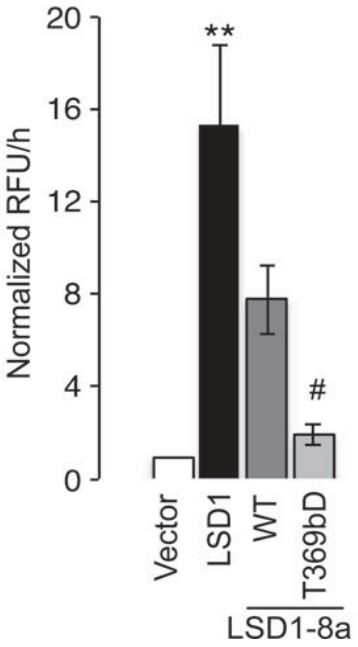

Fig 25 Histone deacetylase assay
Histone deacetylase activity associated to immunocomplexes from HeLa cells, normalized for immunoprecipitation efficiency, expressed as ratio of mock condition. Mean values ± SEM. Statistical analysis revealed significant differences (**p < 0.01 vs. Vector; #p < 0.05 vs. NeuroLSD1). Kruskal–Wallis one-way ANOVA followed by Dunn's post hoc test.

1.3 Phosphorylation of Thr369b alters the local threedimensional structure of NeuroLSD1

In collaboration with the group of Andrea Mattevi, recombinant NeuroLSD1-Thr369bAsp was tandem-affinity purified with CoREST (amino acids 308–440) (Forneris et al. 2007) and its enzymatic properties were evaluated by measuring in vitro demethylase activity using a 21 amino acid monomethylated H3-Lys4 peptide as substrate. We observed no large alterations in the enzymatic functional properties as gathered from the comparison of *k*cat and K_m values (Table 1). We also solved the crystal structure of the mutant protein complex, which indicated no significant overall (including the active site) conformational changes Gly367), with respect to wild-type NeuroLSD1/CoREST (Fig. 24a and b). The room-mean-square deviation calculated from the superposition of the two structures is 0.61 Å for 667 C α atoms. However, the mutation causes a significant alteration in the area surrounding the exon site. In particular, the loop of the Thr369bAsp mutant is shifted up to 5.1 Å (for C α atom of Gly367 remaining fully solvent-exposed. Furthermore, the adjacent a-helix 721–735 also moves by 1.1 Å. These local conformational changes most likely reflect the altered electrostatics associated with presence of the negatively charged Asp side-chain in place of a Thr. They can be especially relevant in light of the hypothesis that exon E8a and the phosphorylation site may influence in vivo the interaction of the phosphorylated protein with its corepressors CoREST, HDAC1, and HDAC2

or may be instrumental to the generation of a properly structured site for recognition of one or more unknown protein partners.

Table 1 Kinetic parameters of the LSD1 and NeuroLSD1 mutants

	*k*cat (min±1)[a]	K_m (μM)[a]
LSD1[d]+CoREST[c]	7.35 ± 0.28[b]	5.12 ±1.04[b]
neuroLSD1[d] + CoREST[c]	5.19 ± 0.48	4.55 ± 1.65
neuroLSD1-T369bD[d]+CoREST[c]	2.44 ± 0.04	3.50 ± 0.30
LSD1-K661A[d] +CoREST[c]	Inactive	–
neuroLSD1-K661A[d] +CoREST[c]	Inactive	–
neuroLSD1- T369bA-K661A[d]+CoREST[c]	Inactive	–

[a]Steady-state kinetic parameters were determined as previously described using a 21 amino acid monomethylated H3-Lys4 peptide (Forneris et al. 2005b). [b]Data taken from Forneris et al. 2007 (Forneris et al. 2007). [c]CoREST from aa 308 to 440. [d]LSD1 from aa 171–840

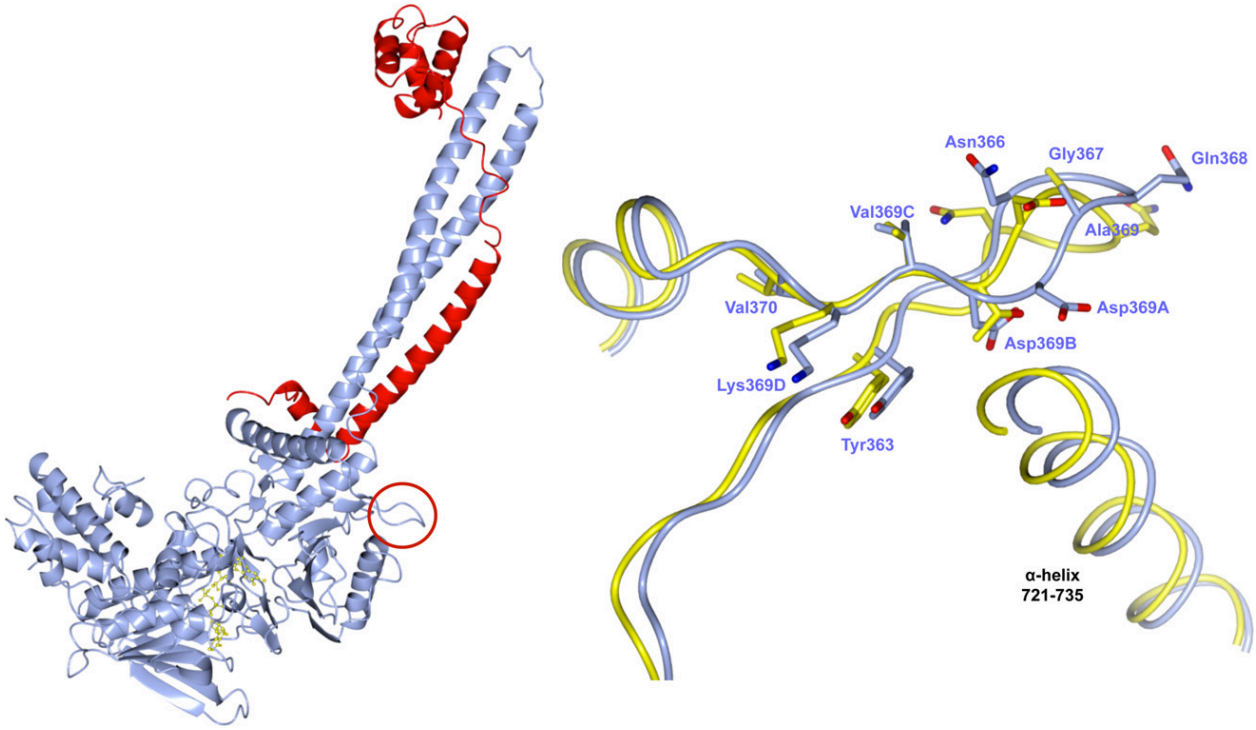

Fig. 24 Structure. (a) Overall crystal structure of neuroLSD1–CoREST Thr369bAsp mutant solved at 3.1 Å resolution (PDB entry 4bay). Mutant NeuroLSD1 (residues 171–840) is colored in blue, whereas CoREST (residues 308–440) in red. The FAD cofactor is shown as yellow ball-and-stick. The insertion site of E8a (residues Asp369a- Thr369b-Val369c-Lys369d) and the site of mutation Thr369bAsp is outlined by a circle. (b) The superposition of the neuroLSD1/CoREST (colored in yellow; PDB entry 2XOL) and neuroLSD1-Thr369bAsp/ CoREST (blue) three-dimensional structures highlights the local conformational change in the residues surrounding the Thr369bAsp mutation. Generated with CCP4 mg (Winn et al. 2011).

1.4 Phosphorylation of neuroLSD1 Thr369b modulates transcriptional repression in neurons

1.4.1 Functional assay

The primary known function of LSD1 is to repress transcription through an epigenetic mechanism based on both histone H3-Lys4 demethylation and recruitment of HDAC1/2 (Shi et al. 2004; Forneris et al. 2005a; Lee et al. 2006a). Consistently, both LSD1 and NeuroLSD1 are capable to repress transcription in neurons. We therefore tested whether phosphorylation, releasing the interaction with HDAC1/2 as well as with CoREST, could hamper the ability of NeuroLSD1 to function as a corepressor in neurons where neuroLSD1 is physiologically expressed. We generated Gal4-neuroLSD1 mutants (Thr369bAsp and Thr369bAla) mimicking a phosphorylated and unphosphorylated status, and evaluated their repressive strength on the basis of the 5X-UAS-TK-Luc reporter gene expression in rat cortical neurons. In each experiment, the promoter activity was measured as luciferase activity normalized over a co-transfected renilla reporter. Repressive strength was inferred through luciferase reduction upon normalization over the promoter activity in the presence of the Gal4 empty vector (Fig 25a, b). Thr369bAsp phospho-mimetic mutation was found to cause loss of repressive activity compared to neuroLSD1 (Fig. 25a; LSD1- 8a-Thr369bAsp vs. neuroLSD1 at 1 : 1 molar ratio 92.45 ± 4.56 vs. 74.49 ± 9.35, $p < 0.05$), becoming similar to the Gal4 empty vector. Conversely, Thr369bAla mutation caused a significant increase in repressive activity compared to neuroLSD1 (Fig. 25a neuroLSD1-Thr369bAla vs. NeuroLSD1 at 1 : 1 molar ratio 53.64 ± 4.23 vs. 74.49 ± 9.35, $p < 0.001$. These data suggest that phosphorylation of Thr369b reduces repressive activity of neuronal neuroLSD1.

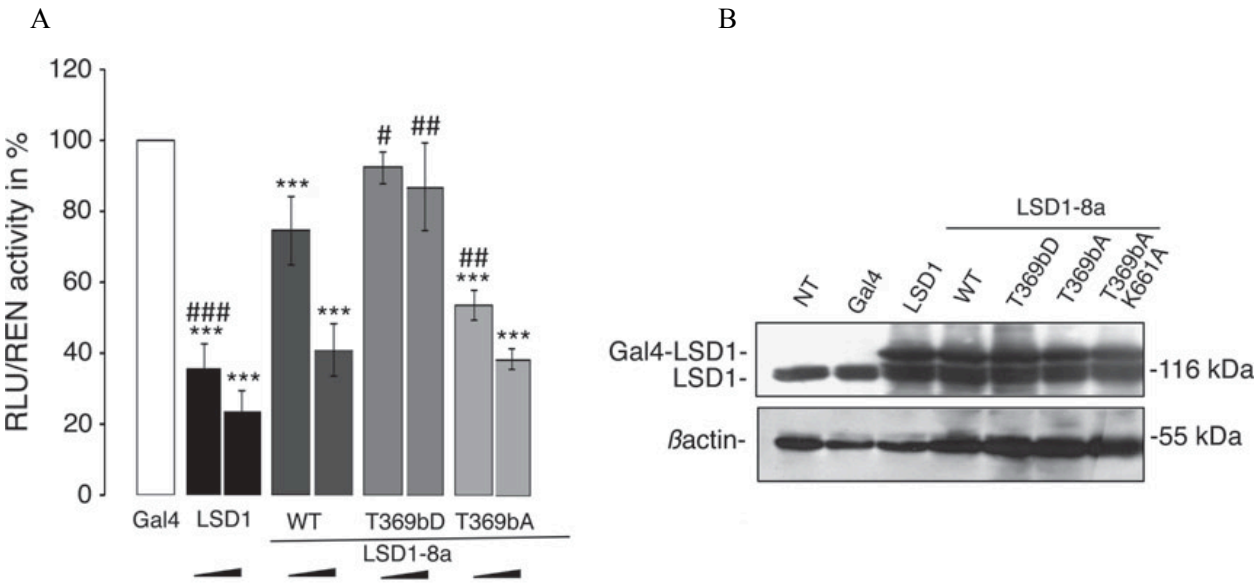

Fig 25 Repressive activity of LSD1s isoforms is modulated by phosphorylation. (A) LSD1 isoforms and mutants fused to Gal4 wereassayed for their ability to repress the 5xUAS-TK-LUC reporter gene in rat cortical neurons at different reporter:repressor molar ratios (1 : 1 and 1 : 2). The luciferase activity normalized on the co-transfected renilla reporter is expressed as a percentage of the Gal4 empty vector. Mean values ± SEM. Statistical analys revealed significant differences (***p < 0.001 vs. Gal4-Vector; #p < 0.05, ##p < 0.01, ###p < 0.001 vs. NeuroLSD1). One-way ANOVA followed by Newman– Keuls' post hoc test. (B) Protein expression levels of LSD1 isoforms and mutant proteins used.

1.4.2 Phosphorylation of NeuroLSD1 modulates gene transcription

To further verify this notion, we infected cortical neurons with lentiviral vectors carrying HA-LSD1, HA-neuroLSD1- Thr369bAsp, HA-neuroLSD1-Thr369bAla, or green fluorescent protein (mock condition) at DIV4 and we analyzed the effect of isoforms over-expression on transcription of selected known HDAC2 brain targets. Indeed, brain HDAC2 plays a central role as negative regulator of complex processes such as memory formation and neuronal maturation (Guan et al. 2009). Total RNA was analyzed at DIV8 by qRT-PCR. We probed genes involved in neuronal maturation and morphology (CDK5R1 and PCTAIRE), neuronal function (GRIN1, PSD95) and two immediate early genes involved in plasticity c-FOS and EGR1, which has already been validated as LSD1 direct target outside the nervous system (Lee et al. 2006b). Transcriptional activity is described as fold gene expression normalized to the housekeeping gene RPSA, relative to mock condition (Fig. 26; similar results were obtained normalizing gene expression to GAPDH as housekeeping, not shown). These experiments gave a clear indication about the opposite effect exerted by phospho-defective and phospho-mimetic mutants.

neuroLSD1-Thr369bAla negatively modulated gene transcription, whereas neuroLSD1-Thr369bAsp over-expression induced up-regulation of the same genes, behaving as a dominant negative isoform. These data are consistent with the reporter gene assays and provide physiological evidence of the phosphorylation role in regulating neuronal morphogenesis through the modulation of morphogenesis-related genes.

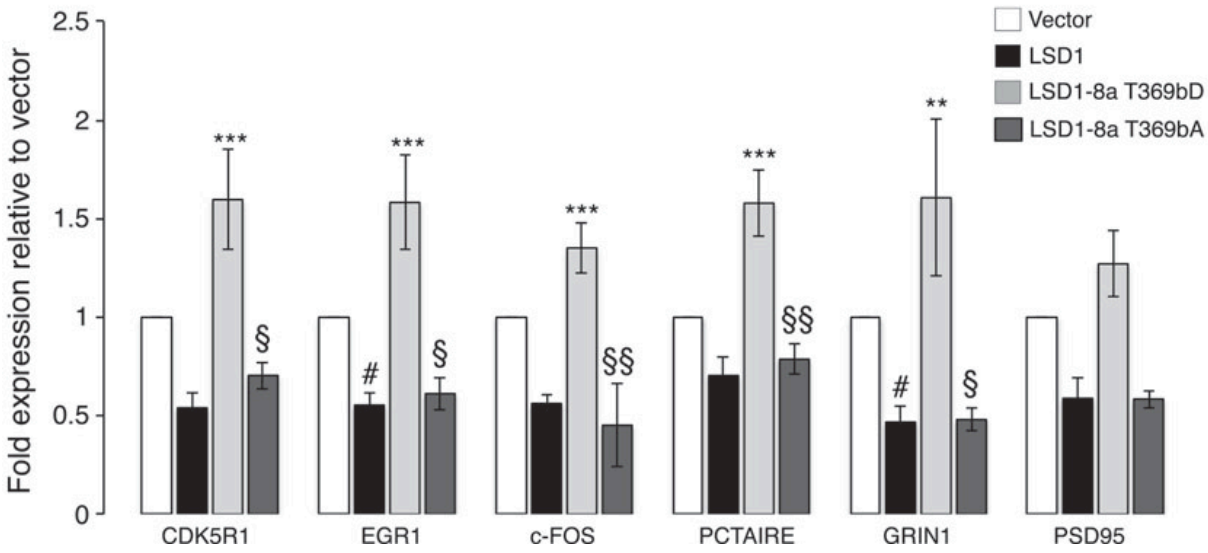

Fig 26 RNA transcripts from cortical neurons after viral transduction with mock, LSD1, neuroLSD1-Thr369bAsp, and neuroLSD1-Thr369bAla for indicated genes (Cdk5R1, EGR1, c-FOS, PCTAIRE, Grin1, PSD95) were quantified by reverse-transcription qPCR. Transcript levels were normalized to RPSA and expressed as the fold expression relative to mock. Pooled data show mean ± SEM. Statistical analysis revealed significant differences (**p < 0.01, ***p < 0.001 vs. LSD1; #p < 0.05 vs. Vector; §p < 0.05, §§p < 0.01 vs. NeuroLSD1-Thr369bAsp). Kruskal Wallis one-way ANOVA followed by Dunn's post hoc test.

1.4.3 Phosphorylation of Thr369b drives morphogenesis in cortical neurons

We previously demonstrated that the presence of exon E8a provides LSD1 with the ability to modulate neurite morphology (Zibetti et al. 2010). On these bases, we asked whether phosphorylation regulates maturation in rat cortical neurons. Based on immunofluorescence and quantitative protein measurements, all enzyme variants over-expressed in cortical neurons showed nuclear localization and similar levels of expression (Figs. 27a, b). In line with previous findings (Zibetti et al. 2010), the neurospecific NeuroLSD1 but not LSD1 had a significant effect on neuronal maturation as evaluated by cumulative neurite length (Fig. 27a and c; mock vs. neuroLSD1, 909 ± 128 lm vs. 1740 ± 64 lm, p < 0.001) and the number of neurite branches (Fig.

30a and d; mock vs. NeuroLSD1, 6.6 ± 1.1 vs. 14.9 ± 1.2, $p < 0.001$). The phospho-mimetic mutant (Thr369bAsp) showed a further tendency to enhance morphogenic effect of neuroLSD1 on cumulative neurite length (Fig. 27a and c; neuroLSD1 vs. LSD1- 8a-Thr369bAsp, 1740 ± 64 μm vs. 1935 ± 50.7 μm) and number of neurite branches (Fig. 27a and d; neuroLSD1 vs. neuroLSD1-Thr369bAsp 14.9 ± 0.7 vs. 17.8 ± 1.2). On the contrary, the phospho-defective mutation Thr369bAla abolished the pro-maturation effect played by neuroLSD1, as no statistical difference could be found when comparing mock conditions with neuroLSD1-Thr369bAla (Fig. 27a and c, neuroLSD1-Thr369bAla vs. mock, 889 ± 45 vs. 909 ± 128 μm; Fig. 27a and d, neuroLSD1-Thr369bAla vs. mock 7.0 ± 0.6 vs. 6.6 ± 1.1) providing further evidence for transfected HA-neuroLSD1 phosphorylation. These data suggest that phosphorylation is indeed necessary to induce morphogenesis in cortical neurons.

Fig 27 Phosphorylation at Thr369b modulates neuroLSD1 morphogenetic properties in neurons. Rat cortical neurons were co-transfected with pCGN vector (mock), HA-LSD1, HA-neuroLSD1, the phospho-mimetic HA-neuroLSD1-Thr369bAsp mutant and the phospho-defective HA-neuroLSD1- Thr369bAla mutant together with pEGFP. (a) Morphological analysis at DIV8 for EGFP- and HA-positive neurons. Scale bars: 20 μm. (b) Protein expression level of wild types and mutant isoforms. (c, d) Quantification of cumulative neurite length and number of secondary branches is indicated ± SEM. ***$p < 0.001$ vs. mock; §§§$p < 0.001$ vs. LSD1; ###$p < 0.001$ vs. HAneuroLSD1-Thr369bAsp. Kruskal–Wallis test oneway ANOVA followed by Dunn's post hoc test was applied to values

A-B

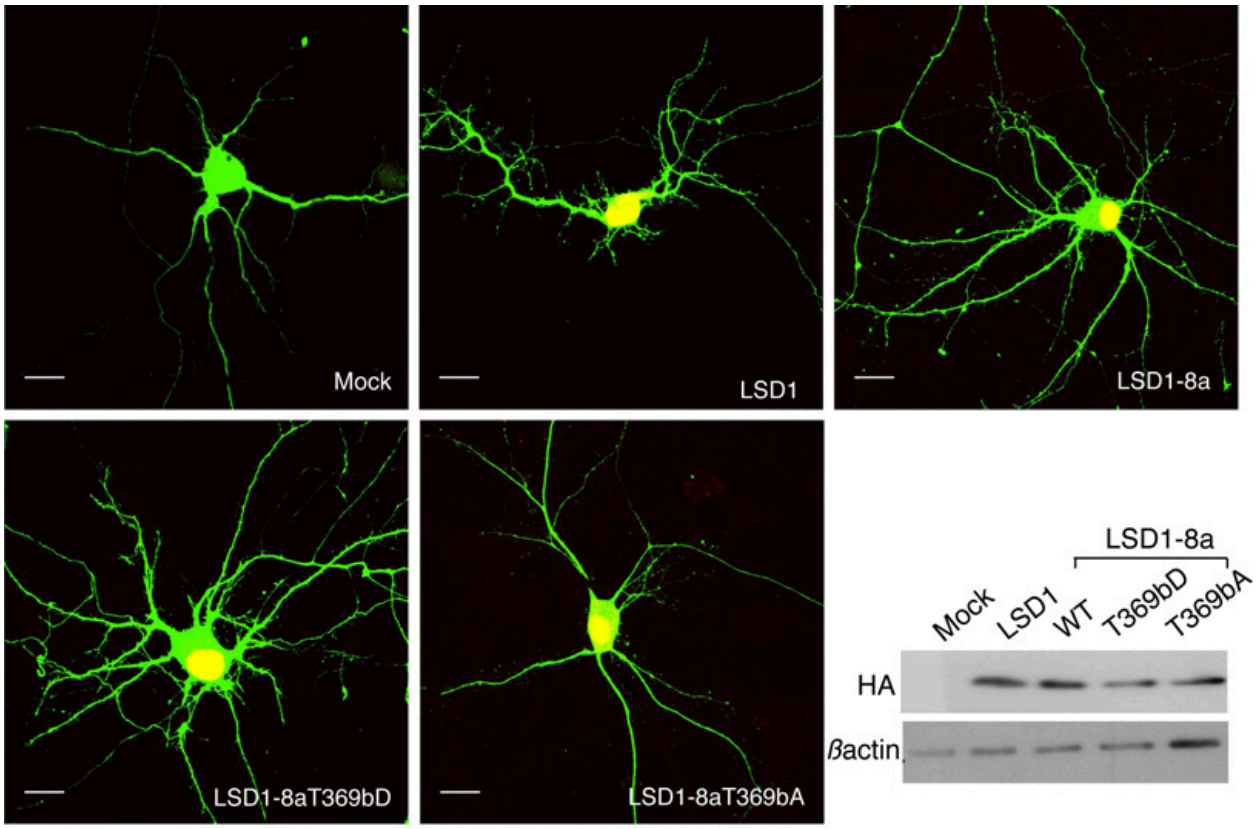
Mock
LSD1
LSD1-8a
LSD1-8aT369bD
LSD1-8aT369bA
LSD1-8a
Mock
LSD1
WT
T369bD
T369bA
HA
βactin

C

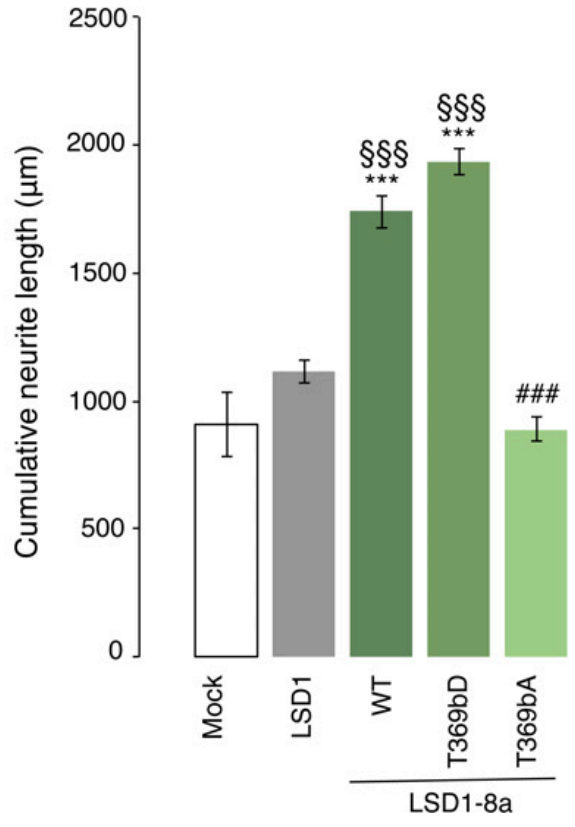
Cumulative neurite length (µm)
2500
2000
1500
1000
500
0
§§§
***
§§§
***
###
Mock
LSD1
WT
T369bD
T369bA
LSD1-8a

D

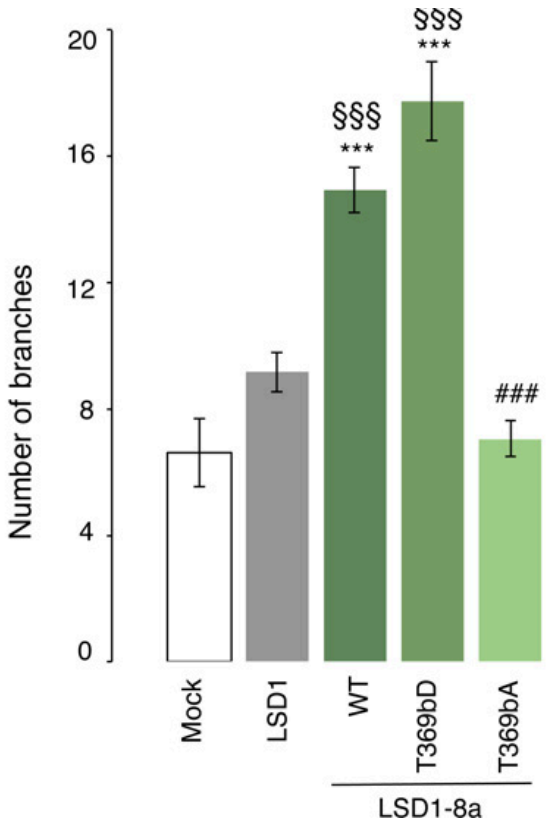
Number of branches
20
16
12
8
4
0
§§§
***
§§§
***
###
Mock
LSD1
WT
T369bD
T369bA
LSD1-8a

1.5 Analysis of the demethylase activity of NeuroLSD1 mutants

The data hereby presented suggest that Thr369b phosphorylation impairs neuroLSD1 mediated transcriptional repression by displacing histone deacetylase activity from the corepressor complex and promoting neuronal maturation and morphogenesis. LSD1 transcriptional repression requires the cooperative action of histone H3-Lys4 demethylation and HDAC1/2 activity (Forneris et al. 2005a; Lee et al. 2005, 2006a; Shi et al. 2005). The evidence that phosphorylation of LSD1 on exon 8a is responsible for the loss of the repressive activity and of further enhancement of pro-maturation effects on rat cortical neurons, prompted us to investigated if it involves the abolition of demethylase activity. We therefore decided to measure the demethylase activity of neuroLSD1-TD (phosphomutant) compared to LSD1 and neuroLSD1. We first tried to assess *in vitro* demethylase activity of the recombinant protein LSD1-TD, as already told at pag. 39 (table 1) and we observed no large alterations in the enzymatic functional properties as gathered from the comparison of kcat and Km values. We then tried an *in vivo* assay using immunopurified complexes from Hela cells overexpressing LSD1 isoforms, as a more phisiologic substrate in wich LSD1 proteins could form in vivo complexes with their cellular parterns. We used a demethylase assay from Epigentek, in wich a di-methylated histone H3-K4 LSD1 substrate is stably coated onto microplate wells. Active LSD1 binds to the substrate and removes methyl groups from the substrate. The LSD1-demethylated products can be recognized with a specific antibody. The ratio or amount of demethylated products, which is proportional to enzyme activity, can then be fluorometrically measured by reading the fluoresence in a fluorescent microplate spectrophotometer at 530 excitation and 590 emission. The activity of the LSD1 enzyme is proportional to the fluorescent intensity measured. The problems we encountered were first due to the low sensivity of the assay, in wich the difference between the blank and the positive control was extremely modest, and the possible differences between LSD1 isoforms demethylase activity not detectable. Secondly, it is possibile that the use of short peptides as substrate represents a limitation. So we tryied to work with nucleosomes as more physiological and informative substrates. We therefore used nucleosome from Hela cells as substrate and immonocomplexes from phosphomimetick mutant expressing Hela cells as source of enzymatic activity. We tried another fluorescent kit (from Active motive- Enzo) but, again, the assay was not enough consistent and sensitive to detect any difference even testing the blank compared to LSD1 condition.

A

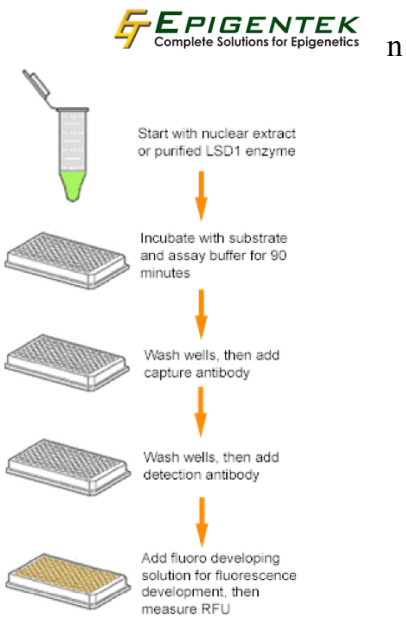

n

B

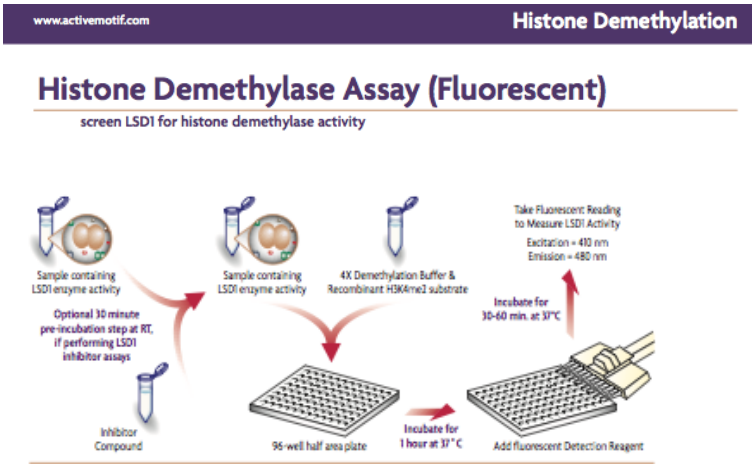

Fig 28 Scheme of Epigentek (A) and of Active-motive demethylase assay (B)

1.5.1 Repressive activity of demethylase null mutants

Since the difficulty in measuring the demethylase activity *in vivo* associated to LSD1, in order to study the relationship neuroLSD1 phosphorylation and demethylase activity *in vivo*, we generated noncatalytic LSD1 and neuroLSD1 mutants. We did it introducing a single mutation (Lys661Ala) in the catalytic site of the protein, already described in leterature to block demethylase activity (see figure 29). We first verify *in vitro* the inactivity of these proteins, and then performed a series of functional assays using rat cortical neurons transiently transfected with this mutated plasmids.

GENERATION OF NONCATALITIC LSD1 MUTANT

Uniprot

Experimental info

☐	Mutagenesis	535	1	N → A: Strongly reduces demethylase activity. Ref.24
☐	Mutagenesis	564	1	H → A: Strongly reduces demethylase activity. Ref.24
☐	Mutagenesis	661	1	K → A: Abolishes histone demethylase activity. Ref.11
☐	Mutagenesis	761	1	Y → A: Strongly reduces demethylase activity. Ref.24
☐	Sequence conflict	78	1	P → Q in AAH40194. Ref.3
☐	Sequence conflict	405	1	P → H in AAH48134. Ref.3
☐	Sequence conflict	669	1	V → A in CAD38675. Ref.4
☐	Sequence conflict	814	1	A → V in AAH16639. Ref.3

Fig 29 Description of the single mutation K661A responsible of the complete abolition of the demethyalse activity of LSD1

We showed that the LSD1-K661A and neuroLSD1-K661A mutants are unable to repress transcription in neurons, since the last mutant reaches a value of luciferase activity almost equal to the mock (Fig. 30, LSD1-K661A vs LSD1: 86,6 ± 1,54 vs 23,4 ± 4,87; neuroLSD1-K661A vs neuroLSD1: 105,23 ± 4,54 vs 40,65 ±4.98).

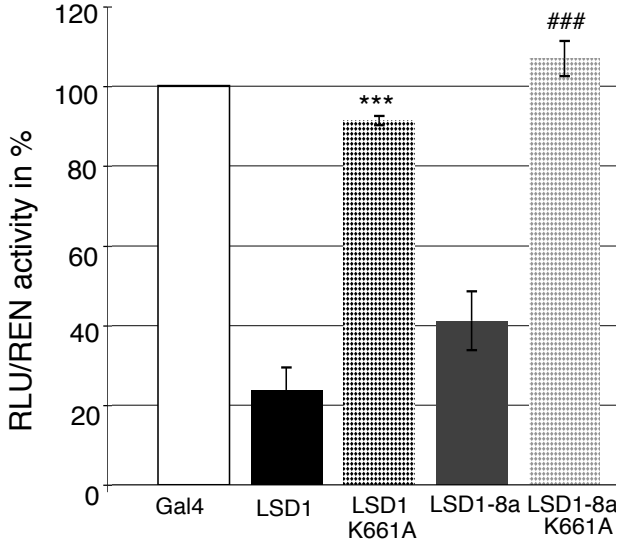

Fig 30 Effect of demethylase inactivating mutation on repressive activity of LSD1. LSD1 and neuroLSD1 fused to Gal4 were assayed for their ability to repress the 5xUAS-TK-LUC reporter gene in rat cortical neurons. The luciferase activity normalized on the co-transfected renilla reporter is expressed as a percentage of the Gal4 empty vector. Mean values ± SEM. Statistical analys revealed significant differences (***$p < 0.001$ vs. Gal4-Vector; #$p < 0.05$, ##$p < 0.01$, ###$p < 0.001$ vs. neuroLSD1). One-way ANOVA followed by Newman– Keuls' post hoc test. (B)

Then we analyzed the ability to these mutants to drive the morphogenesis in rat cortical neurons, comparing LSD1-TD (phosphomimetic mutant) and LSD1-K661A and we found that in this model of neuron maturation, these two mutations have the same effect on cumulative neurite lenght and number of secondary branches (Figure 31).

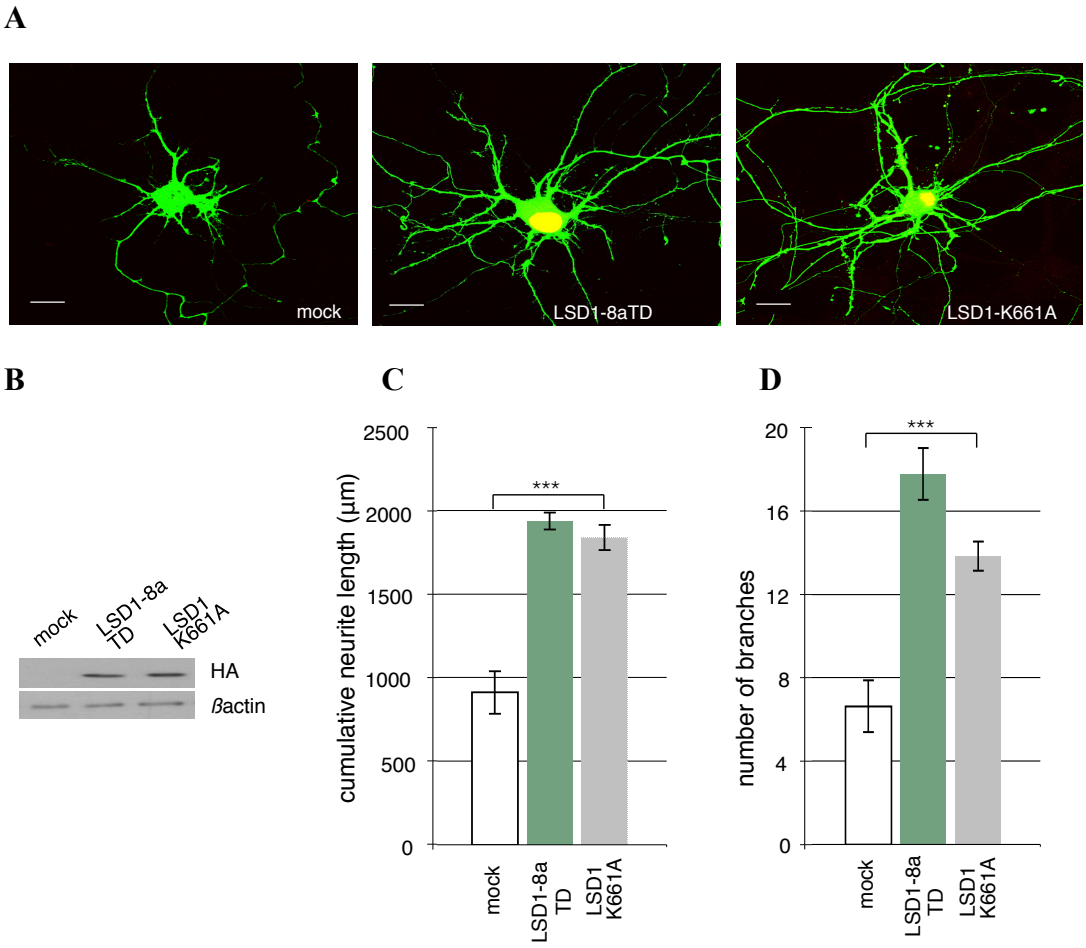

Fig 31 Effect of demethylase inactivating mutation on neuronal maturation in cortical neurons A, Morphological analysis at DIV8 for EGFP- and HA positive neurons. Neurons were co-transfected with pCGN vector (mock), the phospho-mimetick HA-neuroLSD1-Thr369bAsp mutant and the demethylase null HA-LSD1- Lys661Ala mutant together with pEGFP. Scale bars: 20 µm. B, Protein expression level of mutant isoforms. C, D, Quantification of cumulative neurite length and number of secondary branches is indicated ± SEM (***$p < 0.001$ vs. mock). Kruskal–Wallis one-way ANOVA followed by Dunn's post hoc test was applied to values.

Finally, we asked if demethylase inactivating mutation is able to revert the effect of the phospho-defective mutation of NeuroLSD1. So we generated noncatalytic neuroLSD1-TA mutant (neuroLSD1-Thr369bAla/Lys661Ala) and we compared it to neuroLSD1-TA neuroLSD1-Thr369bAla). First, we showed that the neuroLSD1-TA-K661A mutant is unable to repress transcription in neurons, and then we demonstrated that it can partially revert the phenotype of the phospho-defective mutant promoting maturation as shown by cumulative neurite length (Fig. 32c and d; neuroLSD1-Thr369bAla vs. neuroLSD1- Thr369bAla/Lys661Ala 889 ± 45 µm vs. 1530 ± 74 µm, $p < 0.001$) and number of neurite branches (Fig. 32c and e; neuroLSD1-

Thr369bAla vs. neuroLSD1-Thr369bAla/Lys661Ala 7.0 ± 0.6 vs. 12.0 ± 0.8, $p < 0.001$). This result showed that demethylase inactivating mutation is able to phenocopy neuroLSD1 phosphorylation, demonstrating that interfering with the ability of NeuroLSD1 to repress transcription, either by Thr369b phosphorylation or by a demethylase inactivating mutation, promotes neuronal maturation and morphogenesis through a dominant negative effect.

Fig 32 Effect of demethylase inactivating mutation in Lysine-Specific Demethylase 1 (LSD1)-8a on repressive activity and neuronal maturation in cortical neurons. (a) NeuroLSD1-Thr369bAla and a double neuroLSD1-Thr369bAla-Lys661Ala demethylase null mutant, fused to Gal4, were assayed for their ability to repress the 5xUAS-TKLUC reporter gene in rat cortical neurons. The luciferase activity normalized on the co-transfected renilla reporter is expressed as a percentage of the Gal4 empty vector. Mean values ± SEM. Statistical analysis revealed significant differences (**$p < 0.01$ vs. Gal4-Vector; ###$p < 0.001$ vs. neuroLSD1-Thr369bAla). (b) Protein expression level of mutant isoforms. (c) Morphological analysis at DIV8 for EGFP- and HA positive neurons. Neurons were co-transfected with pCGN vector (mock), the phospho-defective HA-neuroLSD1-Thr369bAla mutant and the phospho-defective/demethylase null HA-LSD1- 8a-Thr369bAla-Lys661Ala mutant together with pEGFP. Scale bars: 20 µm. (d, e) Quantification of cumulative neurite length and number of secondary branches is indicated ± SEM (*$p < 0.05$ vs. mock; ###$p < 0.001$ vs. HA-LSD1- 8aThr369bAla). (c–e) Kruskal–Wallis one-way ANOVA followed by Dunn's post hoc test was applied to values.

A

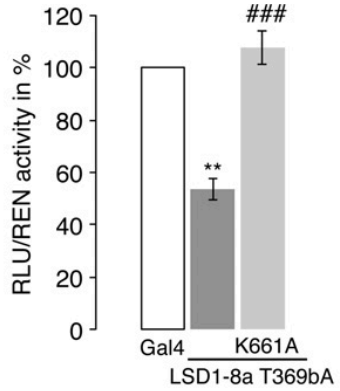
RLU/REN activity in %
120
100
80
60
40
20
0
###
**
Gal4
K661A
LSD1-8a T369bA

B

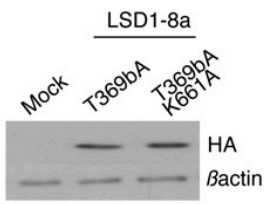
LSD1-8a
Mock
T369bA
T369bA K661A
HA
βactin

C

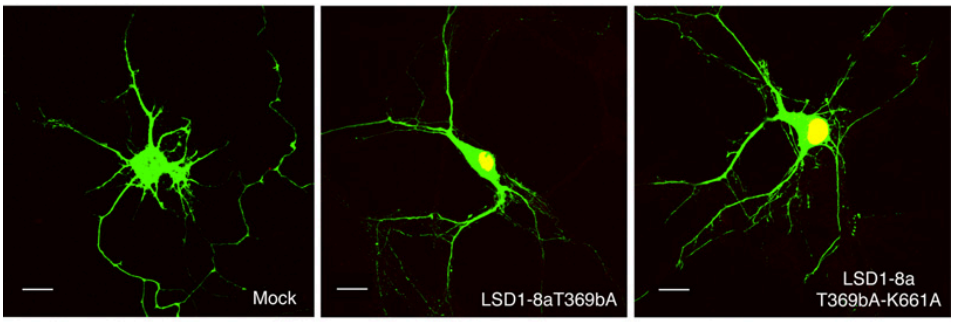
Mock
LSD1-8aT369bA
LSD1-8a
T369bA-K661A

D

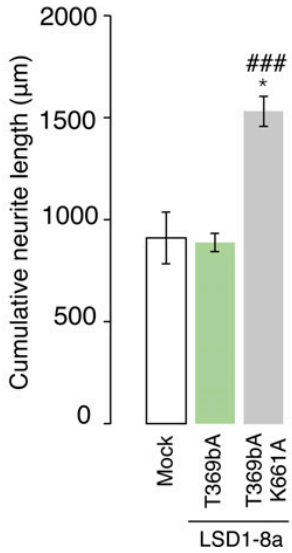
Cumulative neurite length (µm)
2000
1500
1000
500
0
###
*
Mock
T369bA
T369bA K661A
LSD1-8a

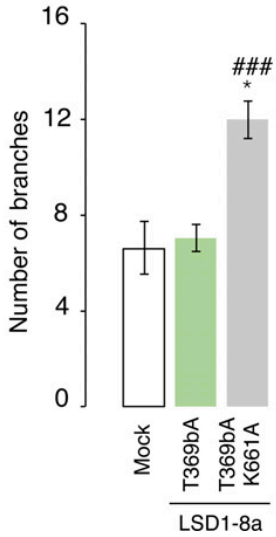
Number of branches
16
12
8
4
0
###
*
Mock
T369bA
T369bA K661A
LSD1-8a

E

1.6 NeuroLSD1 regulates spine density and morphology in hippocampal neurons

Since we observed that overespression of neuroLSD1 is able to enhance neurite morphogenesis (Zibetti et al, 2010) and that this property depends on the phosphorylation of the threonine in exon 8a, we decided to go more indeep into the structures that account for neuronal plasticity, the synaptic spines. Dentritic spines are discrete membrane protrusions present on neuronal dendrites. The highly heterogeneous morphology of dendritic spines is thought to be the morphological basis for synaptic plasticity associated to learning and memory formation. Indeed dendritic spines structure is regulated by molecular mechanisms that are fine tuned and adjusted according to level and direction of synaptic activity, development, specific brain region, and different experimental behavioral conditions. This supports the idea that reciprocal changes between the structure and function of spines impact both local and global integration of signals within dendrites. An increasing number of proteins have been found to be morphogens for dendritic spines and provided new insights into the molecular mechanisms regulating spine formation and morphology. Thus determining the mechanisms that regulate spine formation and morphology is essential for understanding the cellular changes that underlie learning and memory in normal and pathological conditions (Sala et al, 2008). Dendritic spines are essentially formed by a neck and head attached to the dendritic membrane. Most spines have constricted necks and are either mushroom shaped with heads exceeding 0.6 microns in diameter or thin shaped with smaller heads (Harris et al. 1992). Extensive electron microscopy studies of brain tissue have shown that spines can be also stubby, cupshaped or branched protrusions with two or more heads, or single protrusions with multiple synapses along the head and neck (Harris and Kater 1994; Hering and Sheng 2001) and that these different shapes can be found at the same time on the same dendrites (Spacek and Harris 1998). This imperfect classification underlines the multiple forms and dimensions of the spine head and neck providing a way to functionally measure distinct shape categories. Early spines are often very long and have frequent filopodia-like shape but, later during development, their mean length decreases and the number of filopodia is greatly reduced. Three major changes can be observed during the maturation process: an increase in spine density, a decrease in overall length and a decrease in the number of dendritic filopodia with a simultaneous decrease in spine motility.

To analyse the effect of neuroLSD1 on spine density and morphology, we transfected hippocampal neurons at DIV8 with LSD1, neuroLSD1 and vector, together with GFP, and we analyze neurons at DIV18.

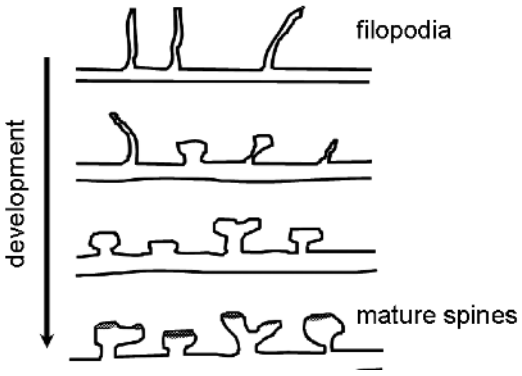

Labelled transfected neurons were chosen randomly for quantification from four coverslips from three independent experiments for each construct. Fluorescent images were acquired with a Zeiss 510 confocal microscope, using a 60X objective with sequential acquisition setting at 1,240 X 1,240 pixel resolution. Image data were a z series projection of about 5–8 images, each averaged 4 times and taken at 0.7µm depth intervals. Morphometric measurements were made with NeuronStudio software. NeuroLSD1 expressing neurons display a significant increase in the number of spines (evaluated as n/10 µm or %) with 0,25-0,30 µm width. neuroLSD1 transfected neurons also display an increase in the percentage of spines with a length comprises between 0,3 and 0,45µm compared to mock neurons. We found a higher number of spines in neuroLSD1 compared to mock condition, but no difference in width and length spines. This analysis shows that neuroLSD1 spines are different from mock for that of middle and small size. This could account for a more plastic condition, in which spines are remodeled in response to different stimuli. We performed this analysis in triplicate, but since the low efficientcy of transfection, other experiments are necessary to improve the number and the statistical significance, and for this reason the results here presented have to be considered preliminary.

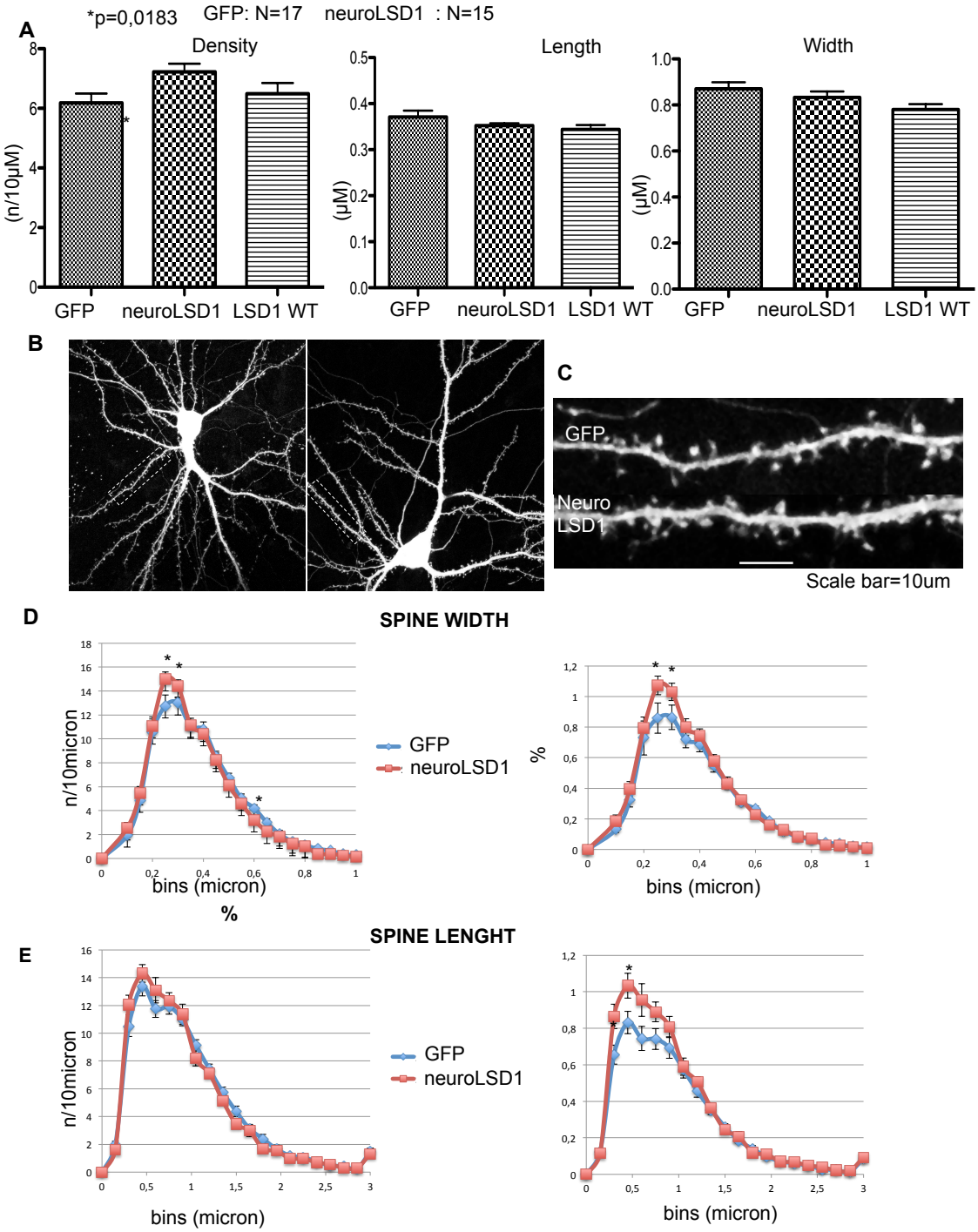

Fig 33 Effect of overespression of LSD1 or neuroLSD1 on hippocampal spine density and size. A) Analysis of spine number (n/10um), width and lenght. B) Morphological analysis at DIV18 for EGFP- and HA positive neurons. Neurons were co-transfected at DIV8 with HA-pCGN vector (mock), HA-LSD1 and HA-neuroLSD1 together with pEGFP but here shown only mock condition (left) and HA-neuroLSD1 (right). Scale bars: 10 µm. C) Particular of a dendrite from mock and neuroLSD1 condition. D,E) Spine distribution according to width and length bins, expressed as density (n/10 µm) or %. We sorted dendritic spines of mock and neuroLSD1 transfected neurons into width and length bins of 0,05 and 0,15 µm respectively. neuroLSD1 expressing neurons display a significant increase in the number of spines (evaluated as n/10 µm or %) with 0,25-0,30 µm width. neuroLSD1 transfected neurons also display an increase in the percentage of spines with a length comprises between 0,3 and 0,45µm compared to mock neurons. All measurements are given as mean standard error of the mean (s.e.m.).

2 IDENTIFICATION OF A NEW TRANSCRIPTION FACTOR RECRUITING LSD1 IN NERVOUS SYSTEM

2.1 Identification of SRF (Serum Response Factor) as molecolar interactor of LSD1 and neuroLSD1

NeuroLSD1 isoform contributes to the acquisition of a proper neuronal morphology, playing an important role *in vitro*, in maturation of rat cortical neurons (Zibetti et al., 2010). Such a phenotype is established by the role of negative dominant of neuroLSD1 towards LSD1 and by the resulting action of derepression on target genes implicated in neuronal maturation and plasticity of nervous cells. Within the LSD1 targets we identified the Immediate Early Genes (IEGs) c-fos and EGR1, and other genes responsible for morphogenesis as CDK5R1 and PCTAIRE. In order to define the role of LSD1 in modulating neuronal plasticy it has been of great importance the identification of SRF as transcription factor regulating the expression of genes aroused by neuronal activity implicated in structural plasticity. The IEGs are target genes of SRF, and several studies have shown as SRF and its targets (c-fos, EGR1, ARC and ΔFosB) are down-regulated in human cerebral samples extracted *post-mortem* from depress patients (Covington et al, 2010; Vialou et al, 2010; Kerman et al, 2012).

SRF is a 508 aa transcription factor containing a MADS box (Knoll and Nordheim, 2009), consisting in a higly conserved and reapeted sequence.This is a zinc- finger protein ubiquitarly expressed and involved in the transcription of a lot of genes. SRF binds to a consensus sequence called CArG-box or Serum Respons Element (SRE), consisting in the motif CC-A/T(6) – GG often found in the promotore or in the first introne of the gene. Thanks to its action on genes involved in the modulation of actin cytoskeleton, it modules spine dynamics and dendrite formation (Knoll and Nordheim, 2009) (Fig 34). It is also important to notice that another SRF target is the neurotrophin BDNF (Essex et al, 2006), involved in synaptic plasticity, dendritic remodeling and important in several neuropathologies (Tsankova et al, 2006).

SRF is a versatile transcription factor, that can operate as a transcriptional activator in stimulus dependent manner and as a repressor in basal condition. However the details of the SRF-mediated genic repression are not yet understood. Since SRF does not include any annotated repressive domain, this kind of function is probably due to the recruitment of epigenetics co-repressors as HDAC4 (Knoll and Nordheim, 2009) or HDAC1/2.

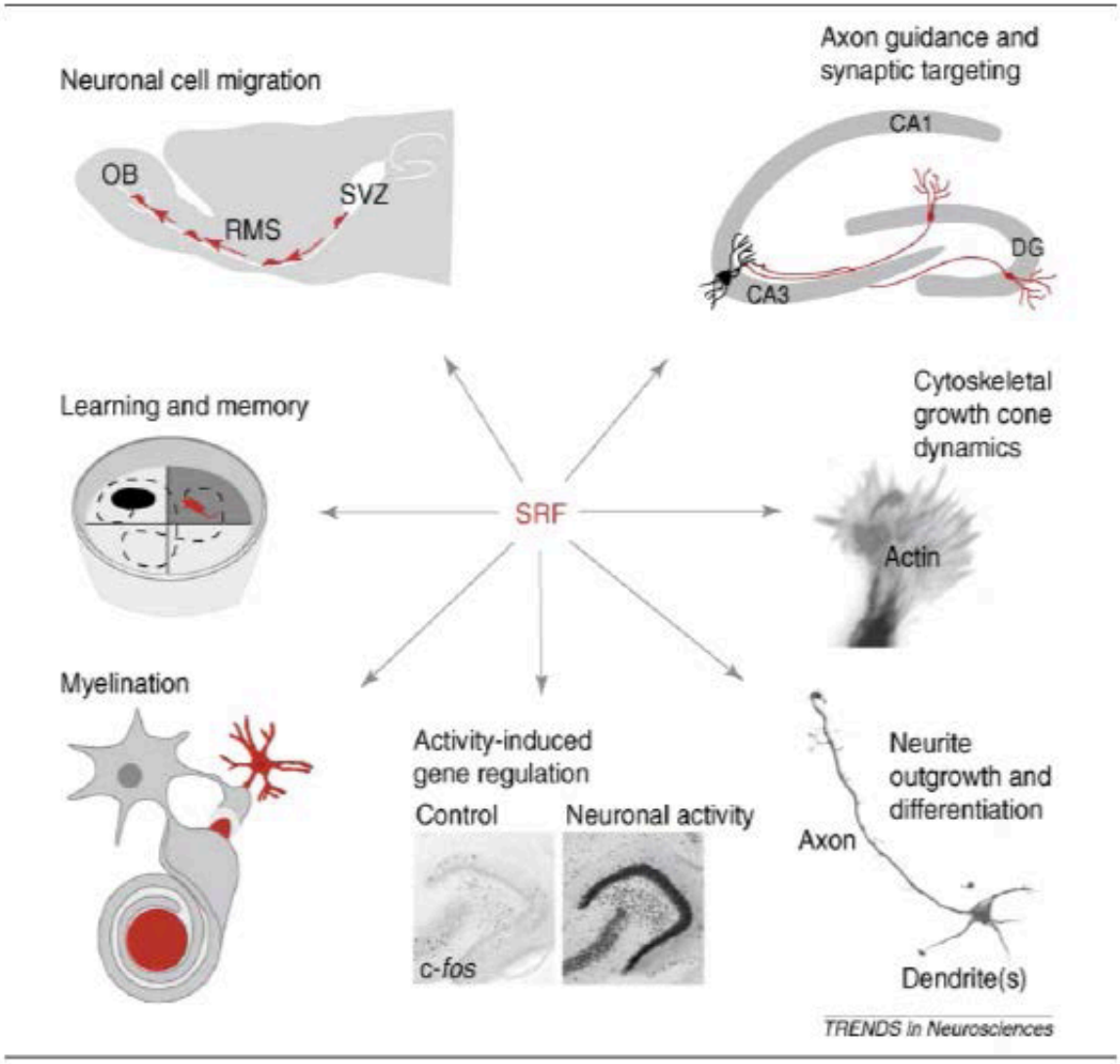

Fig 34 Schematic representation of SRF functions in CNS: SRF modulates neuronal migration, asson formation and synaptic plasticity, as well as the activity-dependent gene transcription (from da Knöll, Nordheim, 2009).

Since the functional convergence beyween SRF and LSD1 and the identification of shared target genes, we hypothesized that the complex conteining LSD1/HDA1/2 could be recruited by SRF complex in "resting" or basal conditions.

Thanks to co-immunoprepitation (CoIP) experiments, we demonstrated the physical interaction between SRF and LSD1 and between SRF and neuroLSD1. Using anti-SRF antibody, we immuprecipitated the two proteins, both *in vitro* in Hela cells (fig. 35B), and *in vivo* in murine hippocampus (Fig. 35A). In particular we performed an *in vivo* experiment in order to study the interaction betwee SRF and LSD1 in murine WT and neuroLSD1^{KO} hippocampi. Using an anti-

SRF primary antibody, and immunodecorating with anti-LSD1, anti-SRF and anti-HDAC2 antibodies, we observed in both genotypes the interaction between the two proteins and the presence of HDAC2, traditionally part of LSD1 repressor complex (Fig 35A). By means of *in vivo* experiments it is not possible to confirm if SRF interacts with both LSD1 and neuroLSD1, as specific antibodies against specific isoforms do not exist. To solve this problem, we performed a communoprecipitation experiment, using Hela cells stably expressing HA-LSD1 or HA-neuro-LSD1, in order to verify if there was any difference in the interaction between the different LSD1 splicing isoforms and SRF. The immuniprecipitates anti-SRF, immunodecorated with anti-HA antibody, showed that both isoforms are tighty associated to endogenous SRF. This interaction could potentially contribute to the versatility of SRF as transcription factor, able to repress transcription in basal conditions, and to activate it in response to stimuli.

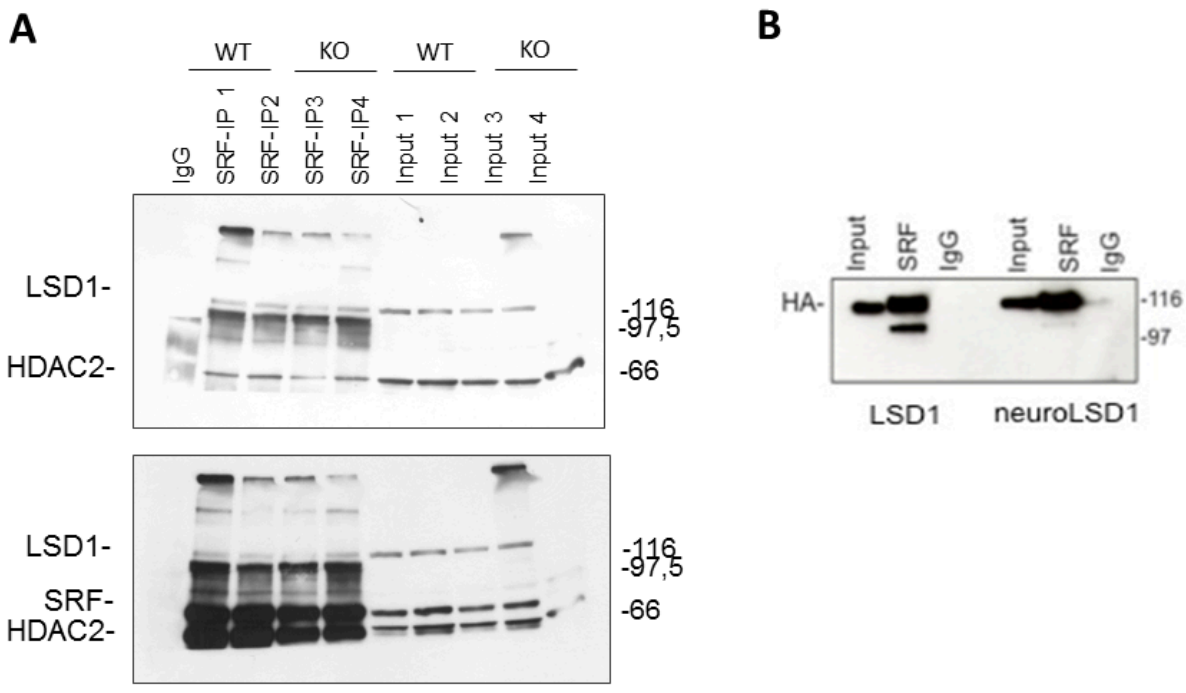

Fig 35 Physical interaction between LSD1 and SRF. A) Western blot analysis of hippocampi proteic samples from WT and neuroLSD1KO mice. IP obtained with anti-SRF antibody and immunodecorated with anti-LSD1, anti-HDAC2 and anti-SRF. B) Western blot analysis of Hela extracts stably expressing HA-LSD1 or HA-neuroLSD1, immunoprecipitetd with anti-SRF and immunodecorated with anti-HA.

2.2 SRF recruits LSD1 and neuroLSD1 to control basal transcription of its targets

Among SRF targets, very important are the IEGs (Knoll, 2011), transcription fators playing a prominent role in neuronal plasticity and memory and learning consolidation in CNS. IEGs are transcription factors that can be sperimentally activated in cellular coltures after a brief acute treatment with high serum (Cen et al, 2004). Egr1 is a protooncoprotein involved in several cellular processes, as growth regulation, transformation, and cellular apoptosis (Thiel, Cibelli, 2002) and it has been demonstrated to be an important promoter of structural synaptic plasticity of hippocampal dentate gyrus, in particular in response to stimuli, as learning. Egr1 is responsive to SFR thanks to the presence in its promoter of five SRE sequences. (Traisman, 1987; Thiel, Cibelli, 2022; Veyrac et al, 2013). c-fos, is another IEG with a transcription factor function, and the first identificated proto-oncogene (Greensberg, Ziff, 1984). Its activation leads to the transcriptional induction of BDNF, that has an important role in activation of genes involved in synaptic remodelling (Kuzniewska et al, 2013). c-fos is responsive to SRF thanks to the presence in its promoter of one SRE sequence (Traisman, 1987). The transcription factor ΔFosB is a IEG is also an onco-protein, with a genic organization similar to c-fos, with several consensus sequences for transcription factors, among wich it is present also a SRE (Lazo et al, 1992). Thanks to the data concerning the molecular interaction between LSD1 and SRF, we wanted to verify if LSD1 was involved also in the transcriptional regulation of SRF target genes, and in particular Egr1 and c-fos, evaluating the interaction of SRF and LSD1 with SRE sites in promoters of mentioned genes. To do this, we performed chromatin immunoprecipitation experiments, from murine hippocampi using ant-SRF and anti-LSD1 antibody. The immunoprecipitated chromatin was submitted to qRT-PCR using specific primers for Egr1 and c-fos promoters. The real time analysis allows a quantitative amplification of immunoprecipitated DNA, necessary for evaluating the presence of the protein on a specific genomic region. The enrichment of the DNA sequences bound to the protein of interest is expressed compared to the mock, that refers to the chromatin immunprecipitated with pre-immune IgG. Primers for Egr1 are drown using Genome Browser UCSC to amplify the regolatory sequences including two of the five CarG box in the Egr1 promoter (Lee et al, 2006), as in figure 36A. Primers for c-fos were designed to include the only one CarG box in the promoter (Traisman et al, 1986), as shown in figure 37B. Data from real time qRT-PCR derived from four distinct experiments, performed in duplicate, on different samples of DNA, extracted from two sonicated and immunoprecipitated chromatins, belonging to different animals. We

found that both in SRF and in LSD1 immunoprecipitated DNA, the promoter sequence of the IEGs was enriched compared to mock condition.. At the level of Egr1, anti-LSD1 immunoprecipitates reveal an enrichment of 2,47 times compared to the mock, whereas anti-SRF immunoprecipitates show an enrichment of 13,66 times over the mock (WT: SRF vs mock: 13,66 ± 9,63 vs 1,00; LSD1 vs mock: 2,47 ± 1,81 vs 1,00. (Fig 37B). Similarly, in c-fos promoter, in anti-SRF immunoprecipitates we found an enrichment of 21,17 times over the mock, whereas in anti-SRF immunoprecipitates we found an enrichment over the mock of 1,42 times (WT: SRF vs mock: 21,17 ± 4,90 vs 1,00; LSD1 vs mock: 1,42 ± 0,29 vs 1,00. (Fig 36D). Moreover, we performed an analysis on a negative control, namely an amplicon derived from the amplification of a region of the promoter Egr1 far away from TSS and lacking of CarG box. In this region we did not find any enrichment neither for LSD1 nor for SRF (WT: SRF vs mock: 0,003 vs 0,015; LSD1 vs mock: 0,001 vs 0,015) (Fig 36E).

In summary, all these data identify SRF as transcriptional factor able to recruit LSD1 on target gene promoter sequences to epigenetically co-regulate their expression. In particular, the identification of LSD1 and neuroLSD1 as SRF interactors in CNS is an important discovery that allows to understand molecular mechanisms through which SRF modules the repression of its target genes.

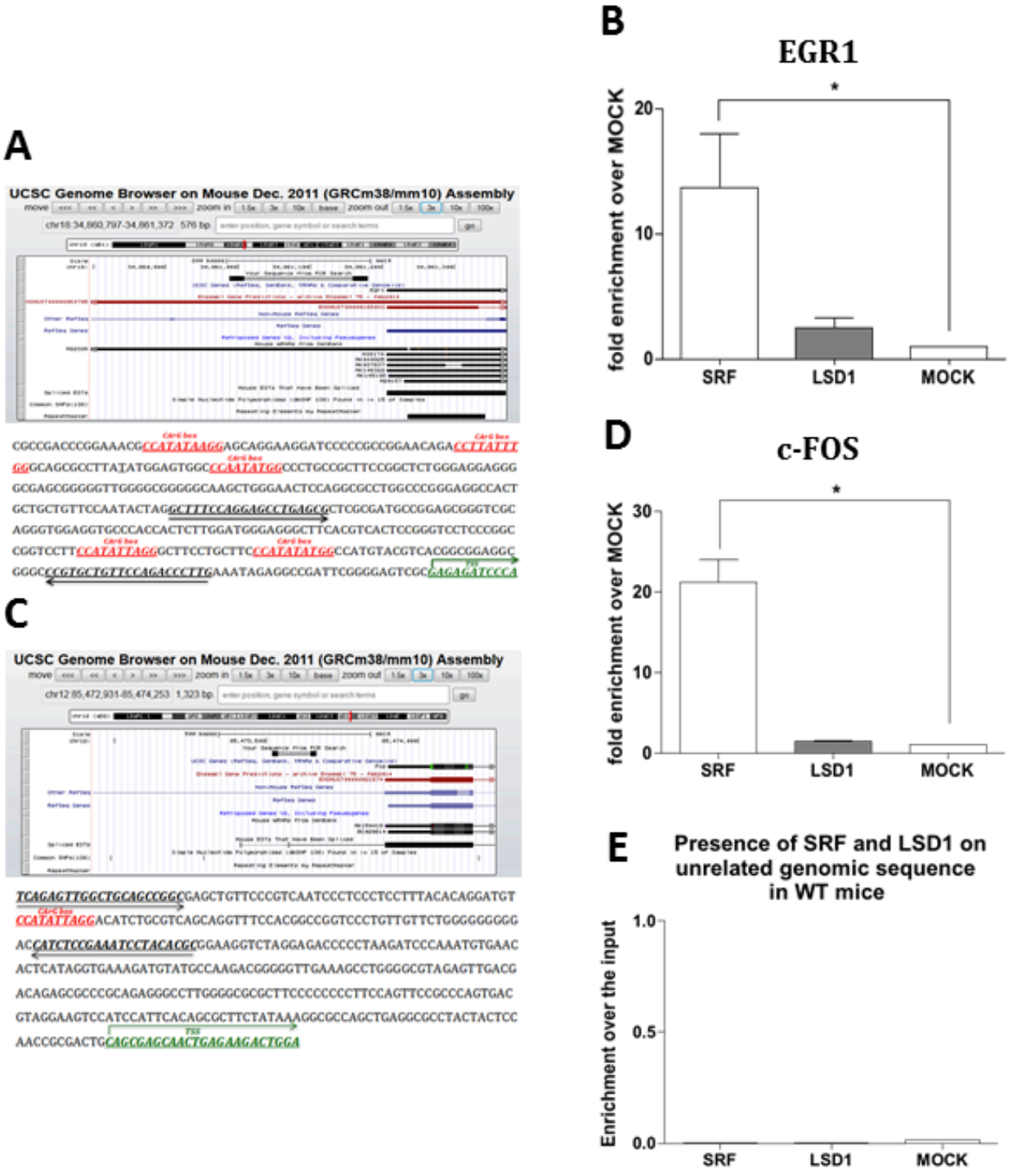

Fig 36 LSD1 and SRF are associated to the chromatin on Egr1 and c-fos promoter. A, prossimal promoter of EGR1 (-434 from TSS), when the five CarG box are in red. Primers in bold. Amplicone 192 bp long. B, D, E, Istograms of the results of the ChIP experiments, performed onEGR1, c-fos and CTRL promoters, using chromatin immunoprecipitated with anti-SRF and anti-LSD1 antibodies. C, prossimal promoter of c-fos (-406 from TSS), when the CarG box is in red and primers in bold. Amplicon 147 bp long. Bars represent error standard. *p≤0,05 Student "t" test.

2.3 Chromatin structure analysis of SRF/LSD1 target promoters

Having demonstrated the physical association between SRF/LSD1 and EGR1 and c-fos promoters, we investigated the contribute of LSD1 demethylase activity in setting a specific chromatin state. We performed ChIP experiments, evaluating the level of dimethyl H3K4 in murine hippocampal tissues comparing wild type with neuroLSD1^{KO} mice. The immunoprecipitated chromatin was submitted to qRT-PCR using specific primers for Egr1 and c-fos promoters, as described before. The enrichment of the DNA sequences bound to the antibody anti-dimethyl H3K4 is expressed compared to the input, that refers to the chromatin not bound to pre-immune. Real time qRT-PCR was performed on DNA samples from chromatin samples derived from at least three different animals. The results showed in figure 37, show that the level of dimethyl H3K4, the LSD1 substrate, is higher in WT mice compared with that of KO mice. On Egr1 promoter, in wild type animals we found an enrichment of 25,16 times over the mock, whereas in KO animals an enrihment of only 4,85 times (EGR1: WT vs WT-mock: 25,16±3,35 vs 1,00; KO vs KO-mock: 4,85±0,85 vs 1,00) (Fig 37A). Similarly, on c-fos promoter, in wild type animals we found an enrichment of 37,53 times over the mock, whereas in KO animals an enrihment of only 3,67 times (c-fos: WT vs WT-mock: 37,53±12,99 vs 1,00; KO vs KO-mock: 3,67±0,78 vs 1,00) (Figura 37B). The amplication of the negative control region (Egr1 ctrl) did not find any specific enrichment in dimethyl H3K4 (WT: SRF vs mock: 0,003 vs 0,015; LSD1 vs mock: 0,001 vs 0,015) and any difference between WT and neuroLSD1^{KO} (Fig 37C).

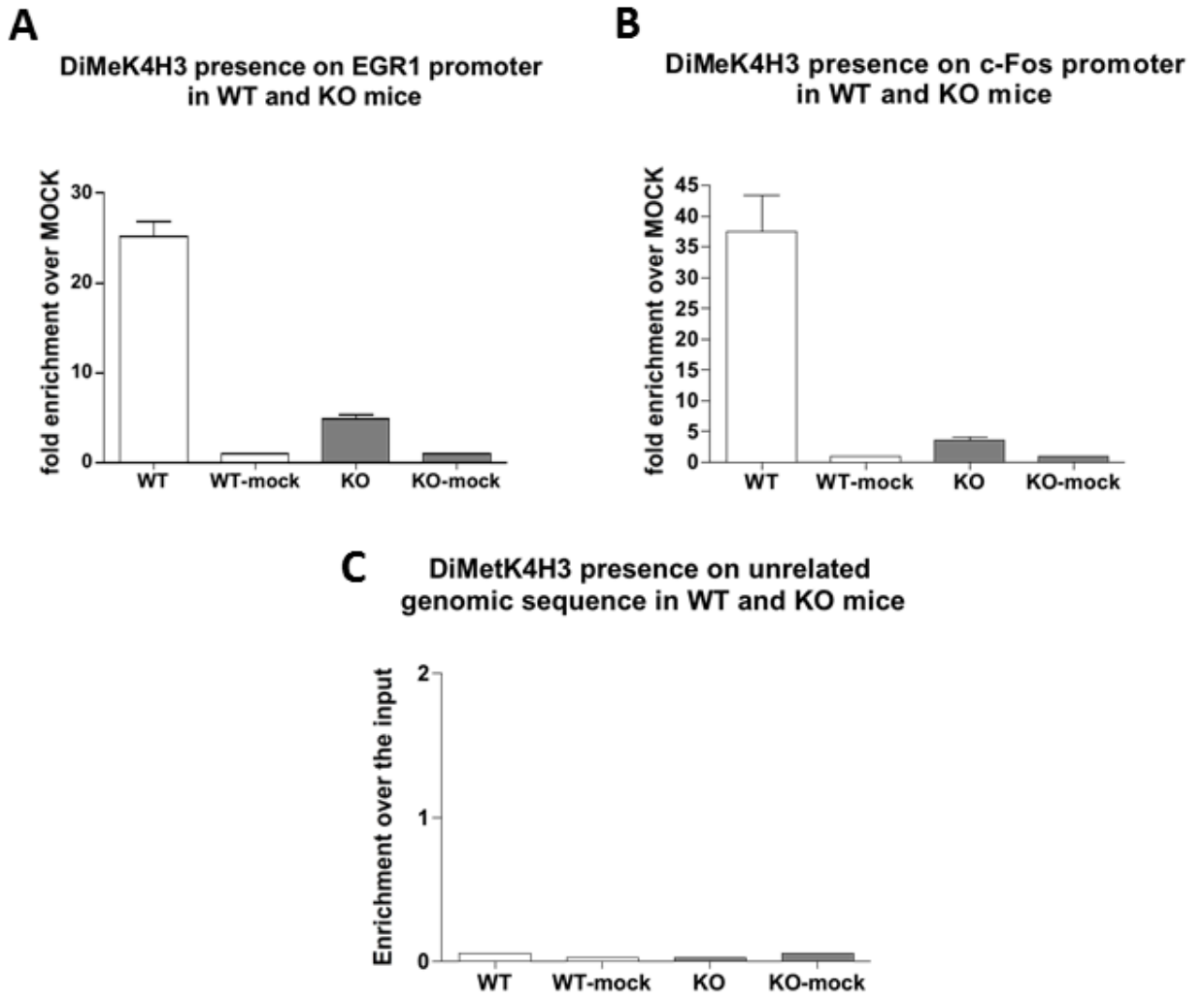

Fig 37 ChIP analysis of the histone 3 Lys 4 dimethylation on Egr1 and c-fos promoters in WT and neuroLSD1^{KO} murine hippocampal tissues. A, B, C, Enrichment of DiMetK4H3 histonic modification on Egr1, c-fos and CTRL proximal promoters. Bars represent error standard.

DISCUSSION

The results we obtained in this work allowed us to highlight the physiological relevance of post-transcriptional (alternative splicing) and post-translational (phosphorylation) mechanisms regulating LSD1 epigenetic activity in the brain in response to neuronal activation modulating the relative levels of LSD1, neuroLSD1 and phospho-neuroLSD1. Furthermore, we identified the the Serum Response Factor (SRF) as new transcription factor recruiting the LSD1/CoREST/HDAC1/2 corepressor complex on its specific target genes. Through this interaction, we unraveled part of the transcriptional pathways regulated by LSD1 at the bases of its ability to modulate neuronal plasticity.

We first tried to understand the isoform specific properties enabling neuroLSD1 to modulate transcriptional pathways regulating morphogenesis in neurons. Purifying LSD1 directly from rat brain, we demonstrated by mass spectrometry that a threonine residue coded by exon E8a, Thr369b, can be phosphorylated in vivo. Maturation experiments in cortical neurons provided a perspective on the physiological consequence of neuroLSD1 phosphorylation during neuronal morphogenesis, unraveling that the pro-maturation effect exerted by neuroLSD1 depends on phosphorylation of Thr369b of the transfected protein. Indeed, over-expression in cortical neurons of the unphosphorylable mutant (Thr369bAla) knocks out the neuroLSD1 pro-maturation effect suggesting that part of the neuroLSD1 over-expressed protein must be phosphorylated in vivo. In line with partial phosphorylation of the transfected neuroLSD1 protein, overexpression of the phospho-mimetic mutant (Thr369bAsp) further enhances neuroLSD1 pro-maturation properties. The crystal structure analysis of neuroLSD1 shows that substitution of Thr369b with an Asp side chain leads to a local conformational change, which affects the residues surrounding the phosphorylation site without altering the catalytic pocket and its demethylase activity in vitro. In vivo, using endogenous proteins, we demonstrated that the structural alteration caused by the phospho-mimetic mutation, is functionally relevant. Indeed, neuroLSD1 phospho-mimetic mutant looses the ability to recruit corepressor partners CoREST, HDAC1, and HDAC2. We suggest that complex disassembly could be directly mediated by phosphorylation or that phosphorylation, being instrumental to the generation of a properly structured protein-binding site, allows recruitment of a new interactor, which could directly or indirectly compete for the binding with corepressors. The functional consequence of complex disassembly on repressive activity stems from the tight functional interdependence and synergistic interplay between LSD1-mediated histone demethylation and histone deacetylation (Forneris et al. 2005a; Shi et al. 2005; Lee et al. 2006a) that provides the biochemical bases to

explain how loss of deacetylase activity is *per se* sufficient to impair repression. Indeed, it has been demonstrated that histone deacetylation is required for proper H3-Lys4 demethylation and the enzymatic activity of LSD1 is required for optimal activity of histone deacetylases.. Further proof that the synergistic interplay between demethylase and deacetylase activities is required to repress gene transcription, is that pro-maturation effect can be achieved also by knocking out neuroLSD1 repressive function interfering with its demethylase activity. Indeed, we were able to phenocopy the pro-maturation effect of the phospho-mimetic mutation with a paradigmatic demethylase-null mutant (Lys661Ala) (Lee et al. 2005). In conclusion, thanks to the phosphomimetic and the demethylase-null mutants, we here demonstrate that neuroLSD1-mediated repression requires both histone H3-Lys4 demethylase and deacetylase activities to functionally regulate gene transcription and morphogenesis. These findings also underline the dual function of neuroLSD1 as histone demethylase enzyme and as scaffold protein. Phosphorylation, regulating disassembly of neuroLSD1 from its corepressor partners, represents a powerful tool to regulate neuroLSD1 repressive potential. Since over-expression of the phospho-mimetic mutant (Thr369bAsp) in cortical neurons increases target genes transcription, we propose that phospho-neuroLSD1 behaves as a transient dominant negative isoform of neuroLSD1, competing with the endogenous unphosphorylated form for the binding to the chromatin substrate. Signal-dependent displacement of HDAC2 from chromatin has already been described as fine strategy to regulate gene transcription in response to stimuli (Palacios et al. 2010). In particular in neurons, NO production and S-nitrosylation of HDAC2 trigger HDAC2 release from target gene promoters, and the activation of genes that are associated with neuronal development (Nott et al. 2008). In this regard, we suggest that phosphorylation of neuroLSD1, inducing dissociation of HDAC1/2 and CoREST, could account for an additional strategy to get rid of HDAC1/2 from specific targets.

During my theses work a very big effort has been made to identify the kinase acting on neuroLSD1 and to produce specific antibodies directed against neuroLSD1 and its phosphorylated form without conclusive results. In this context, we notice that the bioinformatic tool NetPhosK (http://www.cbs. dtu.dk/services/NetPhosK/) strongly predicts protein kinase C as the likely candidate for Thr369b phosphorylation (Saito & Shirai 2002, Schmalz et al. 1998, Leach et al. 1989), providing a first clue for future studies along this research direction. The key conclusion of the first part of this study is that exon E8a alternative splicing and phosphorylation

of Thr369b coded by the same exon, provide a fine dual mechanism to set the LSD1 repressive potential in the brain. During a specific developmental window, which correlates with neuronal maturation, alternative splicing of exon E8a is dynamically controlled (Zibetti et al. 2010). During the adult life LSD1 and neuroLSD1 reach a specific equilibrium, therefore neuroLSD1 repressive potential could be modulated by external signals promoting phosphorylation or de-phosphorylation. We also found that, upon neuronal activation, exon E8a alternative splicing could respond, increasing or decreasing the total amount of neuroLSD1 and consequently LSD1. In particular we observed an activity-dependent downregulation restricted to exon E8a splicing. To better understand the physiological significance of the neuroLSD1 downregulation observed in wild-type mice upon neuronal activation, it was applied PISE (Pilocarpine induced status epilecticus) paradigm to neuroLSD1^{KO} mice. The analysis revealed a substantial reduction in seizure susceptibility of neuroLSD1-null mice relative to wild-type littermates. Furthermore, LSD1 modulation due to importamt stress event, as one single session of social defeat stress (SDS), was investigated. The decreasing of neurospecific splicing and increasing of transcript and protein, show a clear involvement of LSD1 in response to stress. Neuronal activity controls therefore the neurospecific LSD1 splicing. Several examples of activity or developmentally regulated neuronal splicing factors promote the inclusion of alternative exons, many of which contain regulatory phosphorylation sites (Boutz et al. 2007; Zhang et al. 2008; Lee et al. 2009). Whereas there are numerous examples on the role of PTMs in regulating transcription factor functions (Benayoun and Veitia 2009; Everett et al. 2009), our characterization of the post-transcriptional and post-translational mechanism regulating LSD1 function represents one of the very few cases of epigenetic enzyme modulation by PTMs (Nott et al. 2008; Guan et al. 2009; Caretti et al. 2011). The most fascinating aspect of our findings is that neuroLSD1 is the first example of a mammalian epigenetic enzyme specifically devoted to neurons that is potentially capable of responding to intrinsic or extrinsic cell signals, enabling adaptive transcriptional responses in neurons by modifying chromatin. The neurospecific alternative splicing of exon E8a therefore creates a clade-restricted, developmentally regulated PTM modulatory site that may contribute to the increased complexity of mammalian brain (Barbosa-Morais et al. 2012). The nature of the extracellular signals that modulate the epigenetic landscape in the nervous system during development, learning and memory has just begun to be characterized (Nott et al. 2008; Riccio 2010) and given its specificity, neuroLSD1 phosphorylation and exon E8a alternative splicing represent two models to decipher these pathways.

The last part of the work was aimed at the discovery of the functional role of neuroLSD1 in vivo through the identification of trascription factors able to mediate its pro-maturation and morphogenic proterties. Several genes identified as bona fide LSD1 and neuroLSD1 targets where the Immediate Early Genes Egr1 and c-Fos. These genes where downregulated in response to LSD1 overexpression and derepressed by overexpression of a phospho-mimetic mutant of neuroLSD1. Both thses genes are known to respond to stimuly through the activity of two transcription factors, CREB and SRF. By coimmunoprecipitation and chromatin immunoprecipitation, we where able to identify the transcription factor SRF as LSD1 and neuroLSD1 interactor. To unravel the role of LSD1 and /or neuroLSD1 in SRF-mediated transcriptional regulation of IEG, we studied the chromatin structure of Egr1 and c-Fos in the hippocampus of , neuroLSD1KO mice, in which only the LSD1 isoform is present, and compared its H3K4 dimethylation levels with that of WT mice. The chromatin status of KO mice in the evaluated promoters was found to be less enriched in dimethyl H3K4 compared to neuroLSD1^{KO} mice in agreement with the lack of the dominant negative isoform neuroLSD1. Through this quantitative approach we were able to correlate and explain the increase in transcription of c-fos and EGR1 after overespression of phosphomimetic mutant neuroLSD1-Thr369Asp, with a higher degree of dimethylation of these promoters. These data demonstrate the cooperation of LSD1 and SRF in transcriptional regulation of common target genes in basal conditions and further support the idea of LSD1 as trascriptional repressor and of neuroLSD1 as its dominant negative isoform, unable to recruit epigenetic activities as histone deacethylases, that contribute to transcriptional repression of targets. We still do not know if neuroLSD1 phosphorylation might play an active role in the SRF-mediated transcriptional activation upon stimuli.

In conclusion, the double level of LSD1 regulation, the neurospecific splicing and the specific phosphorylation of exon E8a, makes LSD1 a very peculiar and versatile neuroepigenetic factor, able to mediate the interactions between gene and environment and to carry out a homeostatic role that is at the base of the transcriptional plasticity that translate environmental stimuli into morphological and functional changes.

BIBLIOGRAPHY

Barbosa-Morais NL, Irimia M, Pan Q, Xiong HY, Gueroussov S, Lee LJ, Slobodeniuc V, Kutter C, Watt S, Colak R, Kim T, Misquitta-Ali CM, Wilson MD, Kim PM, Odom DT, Frey BJ, Blencowe BJ (2012) The evolutionary landscape of alternative splicing in vertebrate species. Science 338:1587-1593.

Benayoun BA, Veitia RA (2009) A post-translational modification code for transcription factors: sorting through a sea of signals. Trends Cell Biol 19:189-197.

Borrelli E, Nestler EJ, Allis CD, Sassone-Corsi P (2008) Decoding the epigenetic language of neuronal plasticity. Neuron 60:961-974.

Boutz PL, Stoilov P, Li Q, Lin CH, Chawla G, Ostrow K, Shiue L, Ares M, Black DL (2007) A post-transcriptional regulatory switch in polypyrimidine tract-binding proteins reprograms alternative splicing in developing neurons. Genes Dev 21:1636-1652.

Braunschweig U, Gueroussov S, Plocik AM, Graveley BR, Blencowe BJ (2013) Dynamic integration of splicing within gene regulatory pathways. Cell 152:1252-1269.

Cen B, Selvaraj A, Prywes R (2004) Myocardin/MKL family of SRF coactivators: key regulators of immediate early and muscle specific gene expression. J Cell Biochem 93:74-82.

Chen G, Nguyen PH, Courey AJ (1998) A role for Groucho tetramerization in transcriptional repression. Mol Cell Biol 18:7259-7268.

Cibelli G, Policastro V, Rössler OG, Thiel G (2002) Nitric oxide-induced programmed cell death in human neuroblastoma cells is accompanied by the synthesis of Egr-1, a zinc finger transcription factor. J Neurosci Res 67:450-460.

Cosgrove MS, Boeke JD, Wolberger C (2004) Regulated nucleosome mobility and the histone code. Nat Struct Mol Biol 11:1037-1043.

Covington HE, Lobo MK, Maze I, Vialou V, Hyman JM, Zaman S, LaPlant Q, Mouzon E, Ghose S, Tamminga CA, Neve RL, Deisseroth K, Nestler EJ (2010) Antidepressant effect of optogenetic stimulation of the medial prefrontal cortex. J Neurosci 30:16082-16090.

Culhane JC, Cole PA (2007) LSD1 and the chemistry of histone demethylation. Curr Opin Chem Biol 11:561-568.

Dhavan R, Tsai LH (2001) A decade of CDK5. Nat Rev Mol Cell Biol 2:749-759.

Essex MJ, Kraemer HC, Armstrong JM, Boyce WT, Goldsmith HH, Klein MH, Woodward H, Kupfer DJ (2006) Exploring risk factors for the emergence of children's mental health problems. Arch Gen Psychiatry 63:1246-1256.

Everett L, Vo A, Hannenhalli S (2009) PTM-Switchboard--a database of posttranslational modifications of transcription factors, the mediating enzymes and target genes. Nucleic Acids Res 37:D66-71.

Forneris F, Battaglioli E, Mattevi A, Binda C (2009) New roles of flavoproteins in molecular cell biology: histone demethylase LSD1 and chromatin. FEBS J 276:4304-4312.

Forneris F, Binda C, Vanoni MA, Battaglioli E, Mattevi A (2005) Human histone demethylase LSD1 reads the histone code. J Biol Chem 280:41360-41365.

Forneris F, Binda C, Adamo A, Battaglioli E, Mattevi A (2007) Structural basis of LSD1-CoREST selectivity in histone H3 recognition. J Biol Chem 282:20070-20074.

Foster CT, Dovey OM, Lezina L, Luo JL, Gant TW, Barlev N, Bradley A, Cowley SM (2010) Lysine-specific demethylase 1 regulates the embryonic transcriptome and CoREST stability. Mol Cell Biol 30:4851-4863.

Fu WY, Cheng K, Fu AK, Ip NY (2011) Cyclin-dependent kinase 5-dependent phosphorylation of Pctaire1 regulates dendrite development. Neuroscience 180:353-359.

Graeser R, Gannon J, Poon RY, Dubois T, Aitken A, Hunt T (2002) Regulation of the CDK-related protein kinase PCTAIRE-1 and its possible role in neurite outgrowth in Neuro-2A

cells. J Cell Sci 115:3479-3490.
Harris KM, Kater SB (1994) Dendritic spines: cellular specializations imparting both stability and flexibility to synaptic function. Annu Rev Neurosci 17:341-371.
Hering H, Sheng M (2001) Dendritic spines: structure, dynamics and regulation. Nat Rev Neurosci 2:880-888.
Kerman IA, Bernard R, Bunney WE, Jones EG, Schatzberg AF, Myers RM, Barchas JD, Akil H, Watson SJ, Thompson RC (2012) Evidence for transcriptional factor dysregulation in the dorsal raphe nucleus of patients with major depressive disorder. Front Neurosci 6:135.
Knöll B, Nordheim A (2009) Functional versatility of transcription factors in the nervous system: the SRF paradigm. Trends Neurosci 32:432-442.
Lazo PS, Dorfman K, Noguchi T, Mattéi MG, Bravo R (1992) Structure and mapping of the fosB gene. FosB downregulates the activity of the fosB promoter. Nucleic Acids Res 20:343-350.
Lee JA, Tang ZZ, Black DL (2009) An inducible change in Fox-1/A2BP1 splicing modulates the alternative splicing of downstream neuronal target exons. Genes Dev 23:2284-2293.
Lee MG, Wynder C, Cooch N, Shiekhattar R (2005) An essential role for CoREST in nucleosomal histone 3 lysine 4 demethylation. Nature 437:432-435.
Lee MG, Wynder C, Bochar DA, Hakimi MA, Cooch N, Shiekhattar R (2006) Functional interplay between histone demethylase and deacetylase enzymes. Mol Cell Biol 26:6395-6402.
Lois C, Hong EJ, Pease S, Brown EJ, Baltimore D (2002) Germline transmission and tissue-specific expression of transgenes delivered by lentiviral vectors. Science 295:868-872.
Meaney MJ, Ferguson-Smith AC (2010) Epigenetic regulation of the neural transcriptome: the meaning of the marks. Nat Neurosci 13:1313-1318.
Mosammaparast N, Shi Y (2010) Reversal of histone methylation: biochemical and molecular mechanisms of histone demethylases. Annu Rev Biochem 79:155-179.
Nakano Y, Jahan I, Bonde G, Sun X, Hildebrand MS, Engelhardt JF, Smith RJ, Cornell RA, Fritzsch B, Bánfi B (2012) A mutation in the Srrm4 gene causes alternative splicing defects and deafness in the Bronx waltzer mouse. PLoS Genet 8:e1002966.
Naldini L, Blömer U, Gallay P, Ory D, Mulligan R, Gage FH, Verma IM, Trono D (1996) In vivo gene delivery and stable transduction of nondividing cells by a lentiviral vector. Science 272:263-267.
Nikolic M, Dudek H, Kwon YT, Ramos YF, Tsai LH (1996) The cdk5/p35 kinase is essential for neurite outgrowth during neuronal differentiation. Genes Dev 10:816-825.
Nott A, Watson PM, Robinson JD, Crepaldi L, Riccio A (2008) S-Nitrosylation of histone deacetylase 2 induces chromatin remodelling in neurons. Nature 455:411-415.
Palacios D, Puri PL (2006) The epigenetic network regulating muscle development and regeneration. J Cell Physiol 207:1-11.
Patrick GN, Zhou P, Kwon YT, Howley PM, Tsai LH (1998) p35, the neuronal-specific activator of cyclin-dependent kinase 5 (Cdk5) is degraded by the ubiquitin-proteasome pathway. J Biol Chem 273:24057-24064.
Raj B, O'Hanlon D, Vessey JP, Pan Q, Ray D, Buckley NJ, Miller FD, Blencowe BJ (2011) Cross-regulation between an alternative splicing activator and a transcription repressor controls neurogenesis. Mol Cell 43:843-850.
Riccio A (2010) Dynamic epigenetic regulation in neurons: enzymes, stimuli and signaling pathways. Nat Neurosci 13:1330-1337.
Rusconi F, Paganini L, Braida D, Ponzoni L, Toffolo E, Maroli A, Landsberger N, Bedogni F, Turco E, Pattini L, Altruda F, De Biasi S, Sala M, Battaglioli E (2014) LSD1

Neurospecific Alternative Splicing Controls Neuronal Excitability in Mouse Models of Epilepsy. Cereb Cortex.

Saito N, Shirai Y (2002) Protein kinase C gamma (PKC gamma): function of neuron specific isotype. J Biochem 132:683-687.

Sala C, Cambianica I, Rossi F (2008) Molecular mechanisms of dendritic spine development and maintenance. Acta Neurobiol Exp (Wars) 68:289-304.

Schmalz D, Hucho F, Buchner K (1998) Nuclear import of protein kinase C occurs by a mechanism distinct from the mechanism used by proteins with a classical nuclear localization signal. J Cell Sci 111 (Pt 13):1823-1830.

Shi Y, Lan F, Matson C, Mulligan P, Whetstine JR, Cole PA, Casero RA (2004) Histone demethylation mediated by the nuclear amine oxidase homolog LSD1. Cell 119:941-953.

Spacek J, Harris KM (1998) Three-dimensional organization of cell adhesion junctions at synapses and dendritic spines in area CA1 of the rat hippocampus. J Comp Neurol 393:58-68.

Thiel G, Cibelli G (2002) Regulation of life and death by the zinc finger transcription factor Egr-1. J Cell Physiol 193:287-292.

Tsankova NM, Berton O, Renthal W, Kumar A, Neve RL, Nestler EJ (2006) Sustained hippocampal chromatin regulation in a mouse model of depression and antidepressant action. Nat Neurosci 9:519-525.

Ule J, Darnell RB (2006) RNA binding proteins and the regulation of neuronal synaptic plasticity. Curr Opin Neurobiol 16:102-110.

Veyrac A, Gros A, Bruel-Jungerman E, Rochefort C, Kleine Borgmann FB, Jessberger S, Laroche S (2013) Zif268/egr1 gene controls the selection, maturation and functional integration of adult hippocampal newborn neurons by learning. Proc Natl Acad Sci U S A 110:7062-7067.

Vialou V, Maze I, Renthal W, LaPlant QC, Watts EL, Mouzon E, Ghose S, Tamminga CA, Nestler EJ (2010) Serum response factor promotes resilience to chronic social stress through the induction of DeltaFosB. J Neurosci 30:14585-14592.

Winn MD, Ballard CC, Cowtan KD, Dodson EJ, Emsley P, Evans PR, Keegan RM, Krissinel EB, Leslie AG, McCoy A, McNicholas SJ, Murshudov GN, Pannu NS, Potterton EA, Powell HR, Read RJ, Vagin A, Wilson KS (2011) Overview of the CCP4 suite and current developments. Acta Crystallogr D Biol Crystallogr 67:235-242.

Zhang C, Zhang Z, Castle J, Sun S, Johnson J, Krainer AR, Zhang MQ (2008) Defining the regulatory network of the tissue-specific splicing factors Fox-1 and Fox-2. Genes Dev 22:2550-2563.

Zhang C, Frias MA, Mele A, Ruggiu M, Eom T, Marney CB, Wang H, Licatalosi DD, Fak JJ, Darnell RB (2010) Integrative modeling defines the Nova splicing-regulatory network and its combinatorial controls. Science 329:439-443.

Zibetti C, Adamo A, Binda C, Forneris F, Toffolo E, Verpelli C, Ginelli E, Mattevi A, Sala C, Battaglioli E (2010) Alternative splicing of the histone demethylase LSD1/KDM1 contributes to the modulation of neurite morphogenesis in the mammalian nervous system. J Neurosci 30:2521-2532.